




University of
Stavanger

FACULTY OF SCIENCE AND TECHNOLOGY

MASTER'S THESIS

Study programme/specialisation: MSc in Petroleum Engineering / Drilling	Spring/ Autumn semester, 2018 Open
Author: Catherine Cobbah	 (signature of author)
Supervisor(s): Dan Sui	
Title of master's thesis: An Experimental Study on Thermophysical Parameters of Production Wells and their Applications	
Credits (ECTS): 30	
Keywords: Heat transfer Overall heat transfer coefficient Thermophysical parameters Thermal conductivity Specific heat capacity	Number of pages: 76 Stavanger, 16th July, 2018 date/year

Master's Thesis

An Experimental Study on Thermophysical Parameters
of Production Wells and Their Applications



Universitetet
i Stavanger

Catherine Cobbah

Faculty of Science and Technology University of Stavanger

This thesis is submitted for the degree of

Master of Science

July 2018

Dedication

I would like to dedicate this thesis to my dearest husband Øyvind Rasmussen for being my backbone through these challenging times of combining my thesis work and pregnancy. Also to my baby boy, Ohene Ask Rasmussen who has been calm enough to allow me finish my work.

Acknowledgement

I would like to thank God for the strength and good health he has granted me.

My sincerest gratitude goes to my thesis supervisor, Prof. Dan Sui for giving me the opportunity to work with her on this topic. Her guidance, patience and understanding has immensely assisted me in writing this thesis.

A special mention to Ekaterina Wiktorski, a PhD candidate for all her contribution especially devoting quality time to assist me in the laboratory and making insightful comments about various sections of my thesis work.

Finally, my thanks goes to my colleague, Rashid Shaibu, who has been greatly concerned about the completion of my thesis since I was pregnant during the thesis research period and has offered me encouragement and assistance in my thesis work whenever possible.

Abstract

Transient pressure and temperature behavior in a wellbore develops as hot fluids from the reservoir move upward, exchanging heat with the surrounding formation. Because of heat exchange between the production fluid and surrounding formation, the temperature profile in the wellbore does not remain constant with time. This type of heat transmission is involved in drilling, geothermal wells and in all production and injection operations. In certain cases, quantitative knowledge of wellbore heat transmission is very important. Wellbore components such as tubing, cement, casing and annular fluids play a major role in this heat transmission and to be able to quantify this will require knowledge on the thermophysical parameters of the wellbore components. In this study, experiments were performed using the C-Therm TCi™ thermal conductivity analyzer and Tenney Junior Test Chamber™ to measure the thermophysical parameters of wellbore components, specifically, thermal conductivity, effusivity and specific heat capacity in different temperature conditions. Linear and Polynomial correlations were derived and implemented into a wellbore heat transfer model for a single phase oil production scenario, based on the wellbore heat transfer model presented by Hasan, Kabir, and Wang (2009) [1]. Parameter sensitivity tests show that as the flowrate of the produced fluid increases, the rate of heat loss of the fluid decreases and the rate of fluid temperature reduction is lower for higher production times. It is also shown that Flyash as a cement polymer provides better thermal resistance than the other cement systems (G-class, GGBFS and W50). When crude oil was replaced with distilled water as producing fluid, the water experienced minimal heat loss from the bottom to the surface of the wellbore. The findings from this study are important for material selection for geothermal well design.

Table of Contents

Dedication.....	I
Acknowledgement.....	II
Abstract.....	III
Table of Contents.....	IV
List of Figures.....	VII
List of Tables.....	X
Chapter 1.....	1
1.1 Introduction.....	1
1.2 Scope of Study and Objectives.....	2
Chapter 2.....	3
2 Literature Review.....	3
2.1 Heat Transfer.....	3
2.1.1 Conduction.....	3
2.1.2 Convection.....	5
2.1.3 Radiation.....	6
2.1.4 Overall Heat Transfer Coefficient in Wellbores.....	7
2.2 Thermophysical Parameters.....	9
2.2.1 Thermal Conductivity.....	9
2.2.2 Specific Heat Capacity.....	11
2.2.3 Viscosity.....	11
2.2.4 Density.....	12
2.2.5 Coefficient of Thermal Expansion.....	12
2.2.6 Thermal Diffusivity and Effusivity.....	13
2.3 Dimensionless Numbers.....	14
2.3.1 Nusselt (Nu) number.....	14
2.3.2 Prandtl (Pr) number.....	15
2.3.3 Rayleigh (Ra) number.....	15
Chapter 3.....	17
3 Methodology.....	17
3.1 Introduction.....	17
3.2 Experimental Setup.....	17

3.2.1	Description of Test Equipment	19
3.3	Experimental procedure	22
3.3.1	Testing of Liquids	22
3.3.2	Testing of Solids.....	22
Chapter 4	26
4	Experimental Results and Regression Models	26
4.1	Introduction.....	26
4.2	Cement Properties	26
4.3	Casing Properties	28
4.4	Fluid Properties.....	30
4.4.1	Crude Oil.....	30
4.4.2	Water Based Mud (WBM).....	32
4.4.3	Distilled Water	35
4.4.4	Salt Water.....	38
4.5	Formation Properties.....	41
Chapter 5	43
5	Well Configuration and Temperature Model	43
5.1	Introduction.....	43
5.2	Temperature Model.....	43
5.2.1	Well Configuration	44
5.2.2	Calculation of the Overall Heat Transfer Coefficient for the Different Well Sections	46
Chapter 6	53
6	Sensitivity Analysis	53
6.1	Introduction.....	53
6.2	Base Case.....	53
6.3	Effect of Fluid Flowrate	56
6.4	Effect of Production time	57
6.5	Effect of Cement Type	58
6.6	Effect of Annular Fluid	59
6.7	Effect of Produced Fluid	60
6.8	Effect of Casing/Tubing Material	62
Chapter 7	63
7	Summary of Work and Conclusion	63
7.1	Summary of Work.....	63
7.2	Conclusion	63
7.3	Recommendations for further work.....	64

Bibliography.....	65
Appendix A.....	68
Temperature model.....	68
Appendix B.....	76
Salt water Data.....	76

List of Figures

Figure 2.1: One dimensional heat transfer by conduction	4
Figure 2.2: Heat flow through a series of resistances [8]	8
Figure 2.3: Range of thermal conductivity for various states of matter at normal temperatures and pressure [11].	9
Figure 2.4: The temperature dependence of the thermal conductivity of selected solids [11].	10
Figure 2.5: The temperature dependence of the thermal conductivity of selected gases at normal pressures. Molecular weights (M) of the gases are also shown [11].	10
Figure 3.1: The setup showing the various equipment and components of the thermal conductivity experiment.	18
Figure 3.2: A graph of voltage versus time which reveals how the change in temperature affects conductivity of the TCi sensor [19].	19
Figure 3.3: The sensor and guard ring demonstrating how heat is transferred in one directional plane to the sample [19]	20
Figure 3.4 The high pressure cell assembly with the equalizing tube connecting the pressure relief valve, the pressure gauge and On-Off valve by a Swagelok tubing. (Testing with High Pressure Cell) [20].	21
Figure 3.5 The high pressure cell for liquid tests showing the TCi sensor, fine line and O-ring. (Testing with High Pressure Cell) [20].	22
Figure 3.6 The sample positioned on sensor with no additional weight (A) and with additional weight (B) and a silicon rubber between the sensor base plate and the thermal chamber floor.	23
Figure 3.7: Thermal chamber configuration for automatic temperature control	24
Figure 3.8: Experimental procedure	25
Figure 4.1a: Thermal Conductivity for cement polymers as a function of temperature	27
Figure 4.1b: Thermal Conductivity as a function of temperature (Won et al 2016) [22].	28
Figure 4.2 Thermal Conductivity as a function of temperature for Stainless Steel 316 and Steel ST52	29
Figure 4.3 Thermal Conductivity as a function of temperature for Stainless Steel 316 [24] ..	29
Figure 4.4 Thermal Conductivity as a function of temperature for oil.....	30

Figure 4.5 Thermal Conductivity as a function of temperature for WBM	33
Figure 4.6 Specific heat capacity as a function of temperature for WBM	34
Figure 4.7: Variation in viscosity with temperature for drilling fluid (WBM) [30]	35
Figure 4.8: Thermal conductivity of distilled water.....	36
Figure 4.9: Density of distilled water with temperature [32].....	36
Figure 4.10: Specific heat capacity of distilled water	37
Figure 4.11: Dynamic viscosity of distilled water	38
Figure 4.12: Seawater thermal conductivity vs. temperature (35g/kg) [33].....	38
Figure 4.13: Thermal Conductivity of salt water (salinity =30g/kg) [34].....	39
Figure 4.14: Density of salt water (salinity =35g/kg, P= 1atm) [34]	39
Figure 4.15 Specific heat capacity of salt water (salinity =35g/kg, P= 1atm) [34].....	40
Figure 4.16 Viscosity of salt water (salinity =35g/kg, P= 1atm) [34].....	41
Figure 4.17: Thermal conductivity of formation types.....	42
Figure 5.1: Well configuration [13].....	44
Figure 5.2: Temperature distribution throughout the wellbore cross section for section 1 [13]	47
Figure 5.3: Temperature distribution throughout the wellbore cross section for section 2 [13]	48
Figure 5.4: Temperature distribution throughout the wellbore cross section for section 3 [13]	49
Figure 5.5: Temperature distribution throughout the wellbore cross section for section 4 [13]	50
Figure 5.6: Temperature distribution throughout the wellbore cross section for section 5 [13]	51
Figure 6.1: Temperature profile of wellbore (Basecase)	55
Figure 6.2: Overall heat transfer coefficient against depth for wellbore (Basecase)	55
Figure 6.3: Effect of fluid flowrate on produced fluid temperature.....	56
Figure 6.4 Effect of oil flow rate on the temperature distribution curve in the tubing [36]	57

Figure 6.5: Effect of production time on produced fluid temperature	58
Figure 6.6: Effect of cement type on fluid temperature.....	58
Figure 6.7: Effect of cement type on <i>U_{ti}</i>	59
Figure 6.8: Effect of annular fluid on fluid temperature.....	59
Figure 6.9: Effect of annular fluid on overall heat transfer coefficient.....	60
Figure 6.10: Effect of produced fluid on temperature profile.....	61
Figure 6.11: Effect of produced fluid on overall heat transfer coefficient	61
Figure 6.12: Effect of Casing material on temperature profile	62
Figure 6.13: Effect of casing material on overall heat transfer coefficient	62
Figure B1: Thermal Conductivity of salt water (3.5%).....	76

List of Tables

Table 1: Representative values of convective heat transfer coefficient [11]	6
Table 2: Summary of material type with their required thickness, preparation, temperature range and contact agent	24
Table 3: Thermal conductivity of G-class cement specimen [22].	27
Table 4: Ingredients for the main mixture (WBM)	32
Table 5: Ingredients for the supplementary mixture (WBM)	32
Table 6: Wellbore and casing/tubing dimensions for the well.....	45
Table 7: Description of parameters used in the definition on <i>Uti</i>	46
Table 8: Base case parameters	54

Chapter 1

1.1 Introduction

During drilling, production and injection operations, fluids travel through the wellbore either from surface to bottomhole or vice-versa. As this happens, there is heat transfer between the fluids and the earth due to the difference between fluid and geothermal temperatures. The importance of various aspects of heat transfer between wellbore fluid and the earth has been researched by various authors. For example, in 1937, Schlumberger et al [2]. pointed out the usefulness of fluid temperature measurement. In the early 1950's, Nowak [3] proposed using interpretation of temperature logs to estimate water and gas injection profiles. Noting the utility, Kirkpatrick presented a flowing temperature gradient chart. Lesem et al. (1957) [4] and Moss and White (1959) [5] were however the first to suggest procedures for estimating wellbore fluid temperature.

In production operations, as the fluid rises up the well, its temperature soon becomes considerably higher than the surrounding earth temperature because of the general decline in earth temperature with decreasing depth [6]. The temperature difference between the wellbore fluid and the earth causes a transfer of heat from the fluid to the surrounding earth with consequent decrease in fluid temperature, as well depth decreases. The injection of hot-fluid as a means of oil-recovery method—as in the case of heavy oil, depend upon application of heat to the reservoir by means of a heat-transfer medium heated at the surface. Also when the fluid is injected into the reservoir, it must be ensured that temperature differences between the reservoir and the injected fluid are in sync to prevent issues such as solid deposition. In the case of drilling operations, the weight of the mud is of great importance to prevent problems such as kicks and lost circulation which could lead to downtime or in the worst-case scenario, blowout. Since the density of the mud reduces with temperature, a good mud job would have to take into consideration temperature variations along the wellbore. Clearly, heat losses between the surface and the injection interval—in the case of injection wells, or bottom hole and wellhead—in the case of production or drilling operations could be extremely important to these processes.

According to Hasan and Kabir [7], the loss of heat is not only dependent on the radial distance from the well but also on production or injection time and on the various resistances to heat flow between the hot fluid in the tubing and the surrounding earth. These resistances typically include, the production tubing, drill pipe, cement, casing, annulus and insulations. Hasan and Kabir [7] in 1994 presented a method for estimating wellbore fluid temperature. It allowed for wellbore heat transfer by conduction, convection, and radiation through the materials listed above. The thermophysical properties of these materials play a major role in the temperature profile of fluids moving in the wellbore and as such needs to be taken into consideration during material selection for well design and also temperature simulations for production, drilling and injection wells.

1.2 Scope of Study and Objectives

Fluid temperature enters into a variety of petroleum production–operations calculations, including well drilling and completions, production facility design, controlling solid deposition, and analyzing pressure-transient test data [8]. This current study focuses on thermophysical parameters of typical wellbore barriers as they play an important role in heat loss of fluids.

The objectives of this study are to:

1. Conduct experiments for testing thermal conductivity, effusivity and specific heat capacity of wellbore and annular fluids, casing, cement, tubing, and formation in different temperature conditions.
2. Implement the tested parameters into a temperature model for production wells.
3. Perform a sensitivity analysis of the parameters on wellbore temperature distributions.

Chapter 2

2 Literature Review

2.1 Heat Transfer

Heat transfer is basically the process of transfer of heat from high temperature region to low temperature region. In thermodynamics, heat transfer is the movement of heat across the boundary of the system due to temperature difference between the system and the surroundings. The heat transfer can also take place within the system due to temperature difference at various points inside the system. The difference in temperature is considered to be 'potential' that causes the flow of heat and the heat itself is called as flux [9]. The heat flux is defined as the heat transfer rate per unit area normal to the direction of heat flow. There are three basic modes of heat transfer namely: conduction, convection and radiation.

The dominant heat transfer modes in a wellbore are convection and conduction. Radiation heat transfer is usually neglected since the effect is not as significant as the other two modes except if the wellbore annulus is filled with gas. In 2015, the result of Zhou et al [10] indicated that the annulus filled with gas can be utilized as a good thermal barrier for the fluid in the wellbore. By converting the radiation and natural convection into equivalent thermal conduction, their sum is defined as a total thermal conductivity to describe the heat transfer in the annulus.

2.1.1 Conduction

Thermal conduction process occurs at the molecular level where more energetic molecules, being in constant and random motion, periodically collide with molecules of a lower energy level and exchange energy and momentum. In solids the energy transfer is partially due to lattice vibrations mechanism and mostly due to the motion of free electrons, like molecules in gases whiles in fluids the temperature gradient will change as the highly vibrating particles collide with nearby lower energy particles. In liquids, the molecules are closely spaced, and the molecular force field is stronger but in gas the force field is very weak.

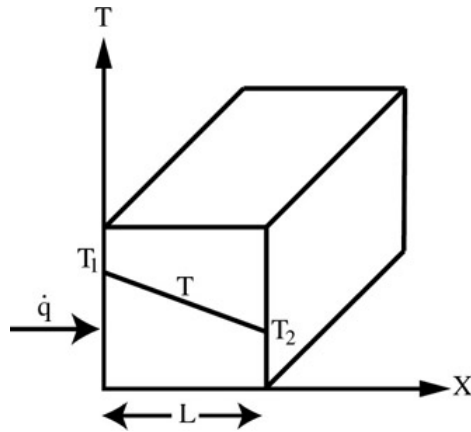


Figure 2.1: One dimensional heat transfer by conduction

In one dimensional form as shown in Figure 2.1, thermal diffusion is governed by the Fourier's law where heat flux q'' [Wm^{-2}] is proportional to the temperature gradient as :

$$q'' = -k \frac{dT}{dx} \quad \text{Eq. 2.1}$$

where k [$Wm^{-1}K^{-1}$] is thermal conductivity, a proportionality constant of the substance; $\frac{dT}{dx}$ is the temperature gradient in x-direction [Km^{-1}]. The direction of the heat flow results in the negative sign.

The heat transfer across the whole length of the plane, L , is then given as:

$$\frac{T_2 - T_1}{L - 0} = -\frac{T_1 - T_2}{L} = -\frac{\Delta T}{L} \quad \text{Eq. 2.2}$$

Where L = length of plane

T_1 and T_2 = temperatures at opposite ends of the plane

ΔT = temperature difference across the plane

The heat transfer equation then becomes:

$$Q = -kA \frac{\Delta T}{L} \quad \text{Eq. 2.3}$$

Where Q = heat rate [W]

A is the area of the surface normal to the direction heat is transferred (m^2)

Bergmann et al [11] in 2011 generated the heat rate conducted through a cylindrical geometry such as pipe or tubing with internal radii r_1 and r_2 being the external radius as:

$$Q = -\frac{kAdT}{dr} = -2\pi rLk \frac{dT}{dr} \quad \text{Eq. 2.4}$$

The eventual heat rate, Q , equation after integrating becomes:

$$Q = \frac{2\pi Lk(T_1 - T_2)}{\ln\left(\frac{r_2}{r_1}\right)} \quad \text{Eq. 2.5}$$

In oil wells, heat transfer by conduction occurs across the tubing walls, cement and casing and any other solid barriers that may be present.

2.1.2 Convection

Convection is the mechanism of heat transfer between a flowing fluid and a solid body or between a gas and a liquid at rest. Convection occurs as a result of bulk fluid motion. Newton in 1709 developed an equation, suggesting that cooling by the convective process is:

$$\frac{dT_{body}}{dt} \propto T_{body} - T_{\infty} \quad \text{Eq. 2.6}$$

The basic heat transfer relation for convection is:

$$\dot{q} = h_c A dt \quad \text{Eq. 2.7}$$

where \dot{q} is the heat transfer per unit time [W], h_c is the convective heat transfer coefficient of the process [$\text{W}/\text{m}^2 \text{ } ^\circ\text{C}$] which varies with the type of flow either being turbulent or laminar, the geometry of the system, the physical properties of the fluid, the average temperature, the position along the surface of the body, and time

The two mechanisms of convection heat transfer are diffusion and advection. While diffusion is the net movement of particles from high to low concentration, advection is the motion of particles along the bulk flow.

Convection heat transfer can be caused when fluid flow is induced by external force or buoyancy forces due to density differences caused by the temperature variations in the fluid. The former is known as forced convection while the latter free or natural convection. The h_c also depend on either natural or forced convection. All the mechanisms makes the determination of h_c hectic. Representative values of h_c is given in Table 1. In well bores, heat transfer by convection is typically through the wellbore fluids and annular fluids [7]

Table 1: Representative values of convective heat transfer coefficient [11]

Condition	h ($\text{W m}^{-2} \text{K}^{-1}$)
Free convection, air	6 – 35
Forced convection, air	28 – 851
Free convection, water	170 – 1140
Forced convection, water	570 – 22 700
Boiling water	5 700 – 85 000
Condensing steam	57 000 – 170 000
Forced convection, sodium	113 000 – 227 000

2.1.3 Radiation

Thermal radiation is the electromagnetic radiation emitted by a body due to its temperature. Among the other forms of electromagnetic waves, it is the only form that is emitted by a body due to its temperature. A distinguishing factor of radiation heat transfer to other heat transfer modes is that, no intervening medium is required between two objects for radiation exchange to occur. It is the only form of heat transfer that can occur most effectively in vacuum.

The energy travels by electromagnetic wave, which is selectively scattered or absorbed in contact with an obstacle. Essentially every object emits electromagnetic radiation and the strength of the emitted energy is correlated to the internal energy state of the emitter. The three principles of electromagnetic wave transfer are emission, absorption and scattering. Scattering encompasses diffraction, interference, reflection and transmission whereas, absorption and emission can be described quantum electrodynamics (QED). However, for most thermal radiation in engineering, black body can be implemented to correlate the temperature of an object with its emission spectrum and energy.

The heat energy flux termed emissive power is proportional to the fourth power of the absolute temperature; that is, $E \propto T^4$. The Stefan-Boltzmann law of thermal radiation states that, the rate at which energy is emitted from the blackbody is proportional to the fourth power of

the absolute temperature of the surface, T_s , of the blackbody, and proportional to the blackbody surface area, A . [12].

$$Q_{emitted} = \sigma AT_s^4 \quad \text{Eq. 2.8}$$

where σ is the proportionality constant, also known as the Stefan-Boltzmann constant with a value of $5.669 \times 10^{-8} \text{ W/m}^2 \text{ K}^4$. A blackbody may for example be a metal piece coated with carbon black, where this black metal piece approximates the blackbody behaviour described by the Stefan-Boltzmann law [13]. If the emissive power occurs on a small surface in a large enclosure, the surface of emissivity, ϵ , comes to play as shown in the equation below

$$Q_{emitted} = \epsilon \sigma A (T_s^4 - T_{surr}^4) \quad \text{Eq. 2.9}$$

2.1.4 Overall Heat Transfer Coefficient in Wellbores

In a well, radial heat transfer occurs between the wellbore fluid and the formation. There exist various barriers which resist heat transfer and this resistance is a combination of conduction, convection and radiation modes of heat transfer. The overall heat transfer coefficient then comes to play. According to Willhite (1967) [14], the steady-state rate of heat flow across a wellbore Q (Btu/hour) is proportional to the temperature difference between the fluid and the formation, and the cross-sectional area perpendicular to the direction of heat flow. The proportionality factor, called the over-all heat transfer coefficient, represents the net resistance of the flowing fluid, tubing, casing annulus, casing wall and cement sheath to the flow of heat. This is written mathematically as;

$$Q = UA\Delta T \quad \text{Eq. 2.10}$$

where U , is the over-all heat transfer coefficient based on the characteristic area A and a characteristic temperature difference ΔT .

Using Figure 2.2, Hasan and Kabir (2012) [8] defined the overall heat transfer coefficient for production through a single string. Because the resistances are in a series, and therefore additive, they wrote the overall-heat-transfer coefficient (based on tubing inside area) as;

$$\frac{1}{U_t} = \frac{1}{h_{ti}} + \frac{r_{ti} \ln\left(\frac{r_{to}}{r_{ti}}\right)}{k_t} + \frac{r_{ti}}{r_{to}(h_c + h_r)} + \frac{r_{ti} \ln\left(\frac{r_{co}}{r_{ci}}\right)}{k_c} + \frac{r_{ti} \ln\left(\frac{r_{wb}}{r_{co}}\right)}{k_{cem}} \quad \text{Eq. 2.11}$$

r_{ci} = casing inside radius, [ft]; r_{co} = casing outside radius, [ft]; r_{ti} = tubing inside radius, [ft]

r_{to} = tubing outside radius, ft; r_{wb} = wellbore radius, [ft];

k_{cem} = cement conductivity (Btu/hr-ft-°F); k_t = tubing conductivity (Btu/hr-ft-°F)

h_{ti} = tubing convective heat transfer coefficient, [$Wm^{-2}K^{-1}$]

U_t = overall heat transfer coefficient, [$Wm^{-2}K^{-1}$]

This expression can be easily adjusted by adding or deleting resistances as the particular situation demands.

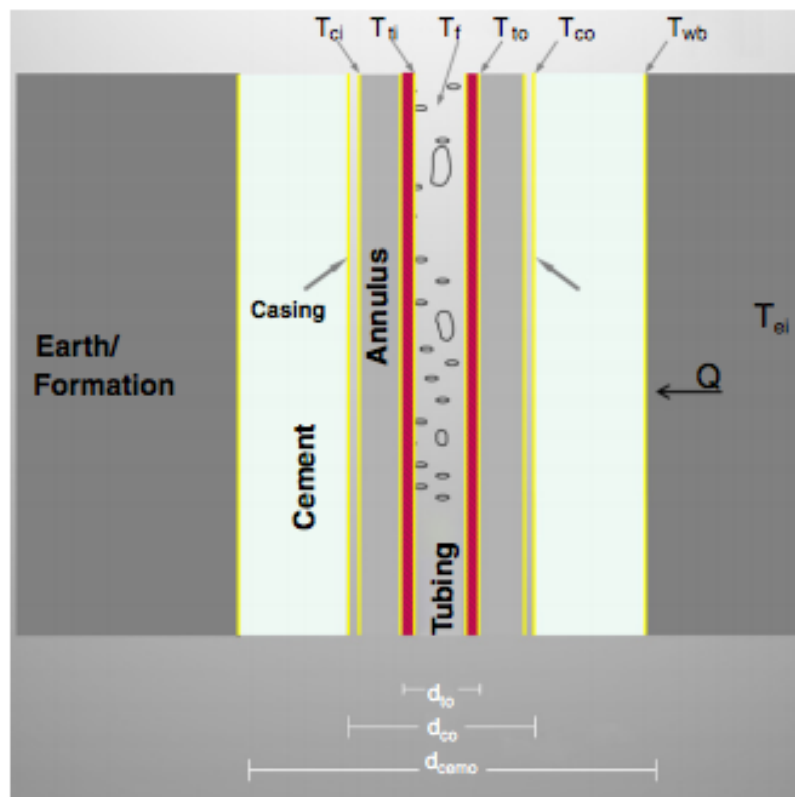


Figure 2.2: Heat flow through a series of resistances [8]

2.2 Thermophysical Parameters

Thermophysical parameters are all material properties affecting the transfer and storage of heat, that vary with the state variables temperature, pressure and composition (in mixtures), and of other relevant variables, without altering the material's chemical identity. These properties will include thermal conductivity and diffusivity, heat capacity, thermal expansion and thermal radiative properties, as well as viscosity and mass and thermal diffusion coefficients [15].

2.2.1 Thermal Conductivity

Thermal conductivities are inherent properties of materials, and they reflect the relative ease or difficulty of energy transfer through the material [11]. According to Fourier's law, (Equation 2.1), thermal conductivity is directly proportional to the heat flux implying increase in heat flux increases thermal conductivity. It is generally known that the thermal conductivity in solids are higher than that of liquid followed by gases this is illustrated in Figure 2.3.

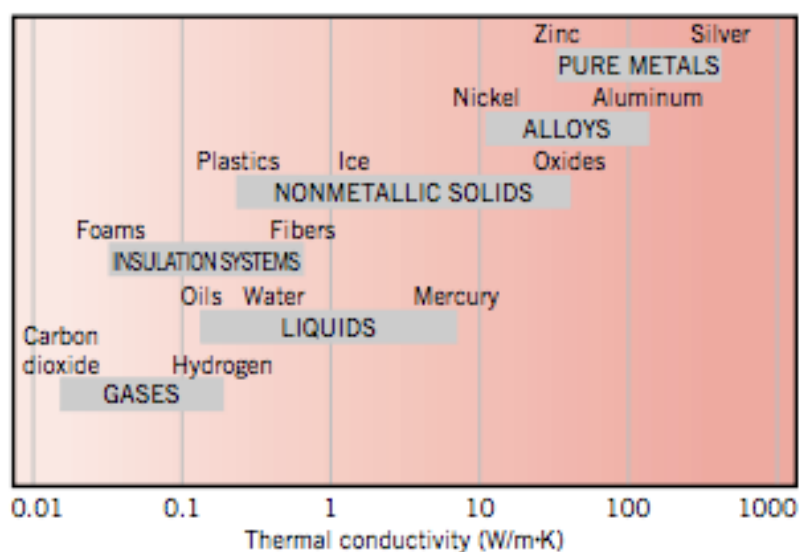


Figure 2.3: Range of thermal conductivity for various states of matter at normal temperatures and pressure [11].

In solids the two modes of thermal energy transfer are by lattice vibration and free electron movement. Metals use both modes while non-metallic use only lattice vibration waves. Figure 2.4 shows the dependence of thermal conductivity on temperature for various metallic and non-metallic solids.

Thermal energy in liquids is transported by kinetic energy exchange. Here the molecules are closely spaced and the molecular force fields are strong. Gases like liquids have the same mode of energy transfer mode but have weak force fields. For ideal gas, it can be proven from the

Kinetic energy of gases that thermal conductivity is proportional to the square root of the absolute temperature;

$$k = \sqrt{T}$$

The dependence of thermal conductivity on temperature for various gases at normal pressure can be seen in Figure 2.5. The inverse of Thermal conductivity is thermal resistivity, W ,

$$W = \frac{1}{k}$$

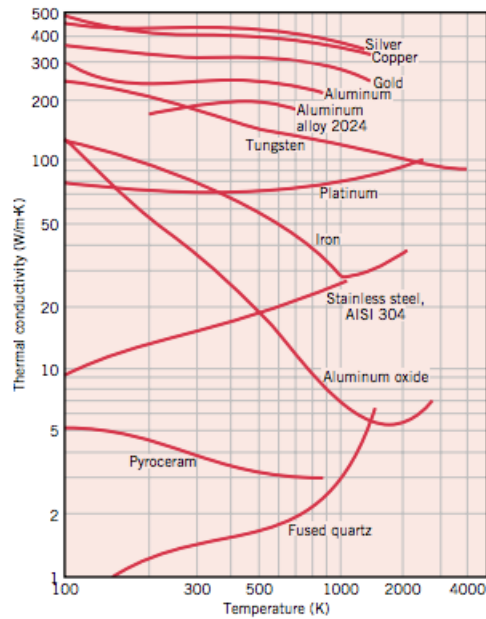


Figure 2.4: The temperature dependence of the thermal conductivity of selected solids [11].

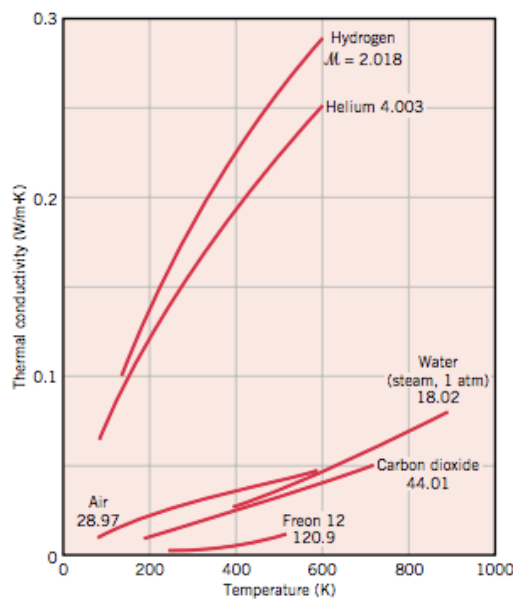


Figure 2.5: The temperature dependence of the thermal conductivity of selected gases at normal pressures. Molecular weights (M) of the gases are also shown [11].

2.2.2 Specific Heat Capacity

Specific heat capacity of a material is the amount of thermal energy needed to change the temperature of a unit mass (m) of a substance by one degree Kelvin. The specific heat capacity term is often used interchangeably with heat capacity which is not accurately right. The specific heat capacity is an intensive property which does not change with size of the system or the amount of the material present in the body while heat capacity is an extensive property of matter that depends on the amount of species in the system and is sensitive to phase changes. The total amount of thermal energy or enthalpy, ΔH , associated with the specific heat capacity and a temperature change (T1 to T2) is given by;

$$\Delta H = \int_{T_1}^{T_2} C_p dT \quad \text{Eq. 2.12}$$

2.2.3 Viscosity

The viscosity is the resistance of the fluid to flow when subjected to an external shear force. The shear stress (τ), or the force per unit area, causing a relative motion of two adjacent layers in a liquid is proportional to the velocity gradient (du/dy), which is normal to the direction of the applied force ($\tau = \eta du/dy$), where the proportionality factor, η , is termed the viscosity. This concept is known as Newton's law of viscosity. Most liquid metals are believed to follow a Newtonian behavior. The unit of viscosity is called Poise (P) ($1P = 1 \text{ dyne s/cm}^2 = 1 \text{ g/cm s} = 1 \text{ mPa s}$). The parameter (η/ρ) is referred to as kinematic viscosity and has units (m^2/s), which are identical to the units for diffusion coefficients and thermal diffusivity. The reciprocal of the viscosity is known as the fluidity. The kinematic viscosity is the ratio of the viscosity to density ($\nu = \eta/\rho$). This is an important parameter in fluid mechanics. The Arrhenius equation is the most common form of representing the temperature dependence of viscosity

$$\eta = A \exp(E_v/RT) \quad \text{Eq. 2.13}$$

where E_v is the activation energy for viscous flow, and R is the ideal gas constant (8.3144 J/K)

2.2.4 Density

Density is another thermophysical property in science in that, it may be used to identify materials, establish relationship between density, thermal, chemical composition and mechanical treatments, etc. Density is defined as the mass per unit volume and usually expressed in grams per cubic centimeter (g/cm^3) at a definite temperature. In some cases, specific gravity is used instead of density since they are both used to express the weight of a substance. Specific gravity is defined as the ratio density of a substance to that of a standard substance. The standard substance for liquid and solid is usually water at 4°C whereas gas is dry air at 0°C.

Generally increasing the temperature of many material increases its volume and thus decreases its density while increase the pressure decreases its volume resulting to an increase in density. For gases, from the ideal gas law, it can be deduced that an increase in temperature results in a decrease in density.

$$PV = nRT$$

In petroleum engineering we usually make use of bulk density, which is basically the density of the porous material and the density of whatever is in the pores.

2.2.5 Coefficient of Thermal Expansion

The coefficient of linear thermal expansion (α) is a material property that indicates the extent to which the material expands or contracts with temperature changes. At a constant pressure, the true coefficient of volumetric thermal expansion (α_v , or commonly β) is defined by the changes that occur by a differential temperature change (∂T). This is usually expressed by the relationship:

$$\alpha_v = \frac{1}{V} \left(\frac{\partial V}{\partial T} \right)_p \quad \text{Eq. 2.14}$$

where V is the volume at a temperature, T, at a constant pressure, P.

The corresponding definition for the linear coefficient of expansion can be represented by the relationship:

$$\alpha_l = \frac{1}{l} \left(\frac{\partial l}{\partial T} \right)_p \quad \text{Eq. 2.15}$$

Usually, the coefficient of thermal expansion is not measured directly but is calculated by the derivative of the equation that represents the expansion. Also, the instantaneous coefficient of linear thermal expansion is frequently defined as the fractional increase of length per unit rise in temperature.

2.2.6 Thermal Diffusivity and Effusivity

Salazar (2003) [16] explained that thermal diffusivity is the quantity that measures the change in temperature produced in unit volume of the material by the amount of heat that flows in unit time through a unit area of a layer of unit thickness with unit temperature difference between its faces. He further explained the physical meaning behind thermal diffusivity as associated with the speed of propagation of heat during changes of temperature over time. It describes how easily heat diffuses through a material, so it depends on thermal conductivity and specific heat. It is expressed mathematically as;

$$\alpha = \frac{k}{\rho C_p} \quad \text{Eq. 2.16}$$

α is the thermal diffusivity (m²/s)

k thermal conductivity (W / (mK))

ρ is the density (kg/m³)

C_p is the specific heat capacity (J/(kgK))

The thermal diffusivity says nothing about the energy flows. On the other hand, the thermal effusivity characterizes the ability to exchange thermal energy with its surroundings [17]. Thermal effusivity is given by the following equation

$$e = \sqrt{\rho C_p k} \quad \text{Eq. 2.17}$$

Where k is the thermal conductivity, ρ is the density and c_p is the specific heat capacity.

In summary, thermal effusivity and diffusivity are characteristic of two phenomena in competition: the former is related to the ability of the material to absorb heat, while the latter to the speed to reach thermal equilibrium, i.e., to adapt itself to the surroundings [17].

2.3 Dimensionless Numbers

In tackling convection heat transfer problems, the common practice is to convert the governing equations to dimensionless equations and combine the variables to dimensionless groups. The Nusselt (Nu) number and its associated Prandtl (Pr), Reynolds (Re) and Rayleigh (Ra) numbers are dimensionless numbers employed in solving convective heat transfer problems.

2.3.1 Nusselt (Nu) number

Nusselt (Nu) number is the ratio of total heat transfer to conductive heat transfer rate.

$$Nu = \frac{\text{Total heat transfer}}{\text{Conductive heat transfer}}$$

$$Nu = \frac{h2r}{k} \quad \text{Eq. 2.18}$$

where h : Conductive heat transfer coefficient [$\text{Wm}^{-2}\text{K}^{-1}$]

r : Pipe wall inside radius at which the heat transfer is considered [m]

k : Thermal conductivity of the fluid [$\text{Wm}^{-1} \text{K}^{-1}$]

Bahrami [18] mentions that, the Nusselt number represents the improvement of heat transfer through a fluid because of convection relative to conduction across the same fluid layer.

$$Nu = \frac{q^*_{conv}}{q^*_{cond}}$$

As defined by Bergmann et al (2011) [11], the Nusselt number is to the thermal boundary layer what the friction coefficient is to the velocity boundary layer. It is a function of the Reynold's number, Re , and the Prandtl, Pr , numbers for forced convection.

Hasan et al., in 2009 [1] also related to the conduction heat transfer coefficient to the Nu for free convection in concentric pipe annulus by :

$$Nu = \frac{h}{k} r_i \ln \left(\frac{r_o}{r_i} \right) \quad \text{Eq. 2.19}$$

where: $r_{(i,o)}$: Inner and outer radius of the annulus [m].

2.3.2 Prandtl (Pr) number

Prandtl (Pr), is a measure of relative thickness of the velocity and thermal boundary layer molecular diffusivity of heat molecular diffusivity of momentum P

$$Pr = \frac{\text{molecular diffusivity of momentum}}{\text{molecular diffusivity of heat}} = \frac{\nu}{\alpha} = \frac{\mu C_p}{k} \quad \text{Eq. 2.20}$$

Where: ν : kinematic viscosity [m^2/s]

α : thermal diffusivity [m^2/s]

μ : dynamic viscosity [$N \cdot s/m^2$]

2.3.3 Rayleigh (Ra) number

The Rayleigh (Ra) number shows how heat is transferred through fluid. The two modes of heat transfer in fluids in the presence of temperature gradient are conduction and convection. The Rayleigh number tells which mode dominates in the fluid. When Rayleigh number exceeds a critical value the dominant mode of transfer is convection whereas if the it is below the critical value the dominant mode is conduction. The Rayleigh number is expressed as:

$$Ra = GrPr \quad \text{Eq. 2.21}$$

Where: Gr = Grashof number, which is the measure of the ratio of the buoyancy forces to the viscous forces in the velocity boundary layer. When comparing two fluids at the same temperature, the more viscous fluid will have restricted movement and thus, a low Grashof number.

Gr is expressed by Bergmann et al. [11] as :

$$Gr = \frac{g\beta(T_s - T_\infty)\rho^2 L^3}{\mu^2} \quad \text{Eq. 2.22}$$

Where: β : Thermal expansion coefficient [k^{-1}]

L : Characteristic length [m]

T_s : Surface temperature [$^{\circ}\text{C}$]

T_∞ : Fluid temperature just outside the boundary layer [$^{\circ}\text{C}$]

g: acceleration due to gravity.

Chapter 3

3 Methodology

3.1 Introduction

This chapter presents a description of the equipment used in the experiments and the procedures followed to obtain the desired data for analysis. In determining the thermophysical properties of typical well components at varying well temperatures, the C-Therm TCi thermal conductivity analyzer and Tenney Junior Test Chamber were used.

The well components considered were the wellbore and annular fluids, casing materials, cement and formation. The fluids considered were distilled water, brine and water based mud. For the casing material, we tested stainless steel 316 and Steel (ST52). Class G cement, Fly ash, W50 and GGBFS polymers were also considered for cementitious barrier whiles sandstone, bentheimer, gray Berea and chalk cores were considered for formation.

The thermophysical properties which includes the effusivity, thermal conductivity, heat capacity, volumetric specific heat, R-value (insulations), depth of penetration are indirect measurements from the C-Therm TCi thermal conductivity analyzer. The properties above are obtained from the direct measurement of the thermal effusivity (thermal inertia) of the material by the analyzer. The analyzer has been calibrated to fit within various material groups for accurate results. In circumstances where the material being tested does not fall within the calibrated material groups with different density and heat capacity range, an unacceptable error will display

3.2 Experimental Setup

The equipment for the experiments consist of a laptop with the C-Therm TCi software installed, C-Therm TCi controller, C-Therm TCi sensor, Contact agents, Reference material kit, C-Therm TCi sensor base, High pressure cell, Power cable and USB cable and a thermal chamber.

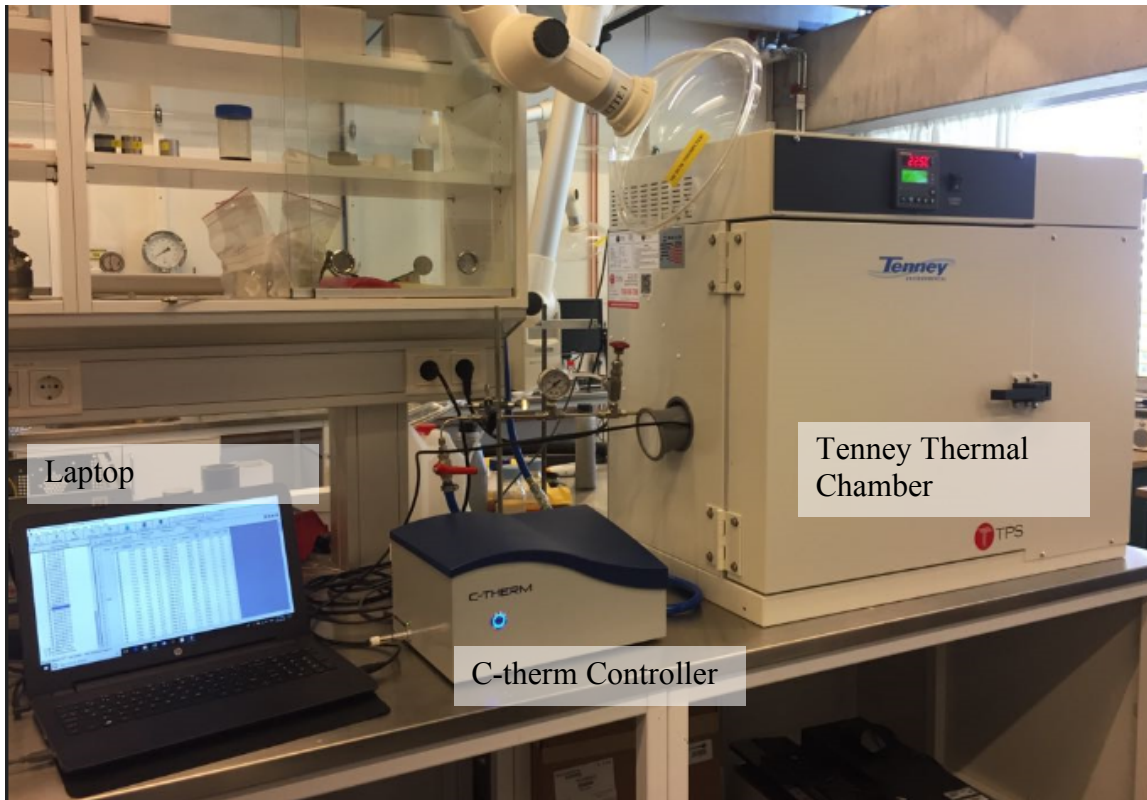


Figure 3.1: The setup showing the various equipment and components of the thermal conductivity experiment.

The C-Therm TCi thermal conductivity analyzer employs the patent of Modified Transient Plane Source (MTPS) technique for the nondestructive measurement of thermal conductivity and effusivity of the samples being tested. The MTPS method is composed a one-sided heat reflecting sensor embedded with a heat element with support from insulative backing and surrounded by a guard ring. This implies only an interface of the sample is required. When a current is applied instantaneously to the sensor and guard ring, heat is generated. With the aid of the guard ring and the supporting insulative backing, the heat is transferred in a one directional plane to the sample. The rate of temperature increase is observed by the voltage drop of the primary sensor coil which is attuned to the temperature change. In figure 3.2 it can be observed that the thermal conductivity of the sample is inversely proportional to the rate of increase to the temperature monitored which means that if the material has a lower the thermal conductivity or is good insulator, the slope of the temperature rise will be steeper as to that of a good conductor. The graph in Figure 3.2 shows a non-linear curve in the first 0.3 seconds whiles the sample is establishing contact and then until the next 0.8 seconds when the heat has been transferred into the sample, a linear curve is obtained.

The thermal chamber put in service when samples need to be tested at elevated temperatures.

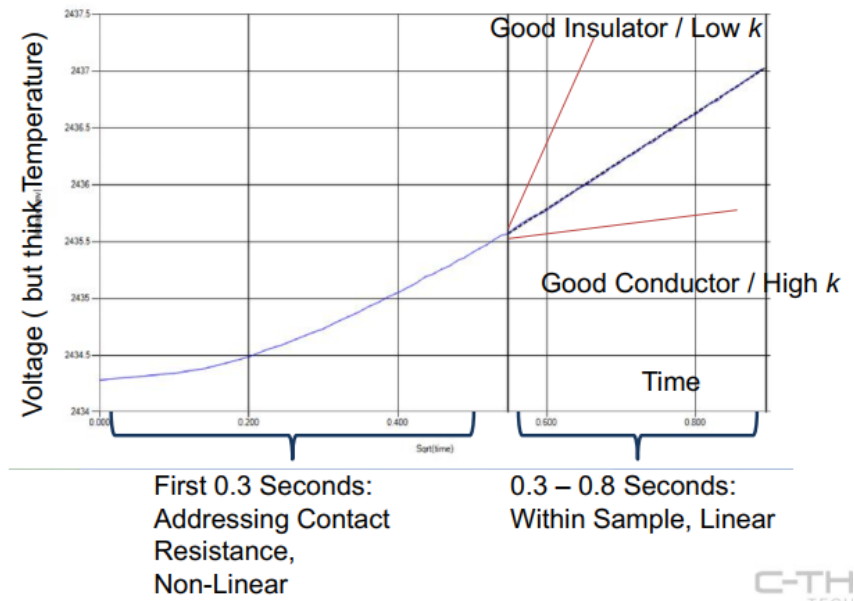


Figure 3.2: A graph of voltage versus time which reveals how the change in temperature affects conductivity of the TCi sensor [19].

3.2.1 Description of Test Equipment

Laptop with the C-Therm TCi software

The laptop has a Windows based software interface where the software includes a full relational database with importing and exporting capability and provides the ability to derive other thermophysical properties such as density and specific heat capacity indirectly with additional inputted data. The software communicates between the thermal chamber and the TCi thermal controller. The temperature change with time of the thermal chamber can be controlled by software or manually on the chamber. Test results is displayed in real time.

C-Therm TCi sensor

The sensor is factory calibrated where calibrations are stored in the database and the sensor chip. Before test were run, calibrations were tested the various reference materials provided in the reference standard to ensure accurate measurements. The sensor employs the MTPS methods is composed of a one-sided heat reflecting sensor embedded with a heat element with support from insulative backing and surrounded by a guard ring. This implies only an interface of the sample is required. When a current is applied instantaneously to the sensor and guard ring, heat is generated. With the aid of the guard ring and the supporting insulative backing, the heat is transferred in a one directional plane to the sample as shown in figure 3.3. The rate

of temperature increase is observed by the voltage drop of the primary sensor coil which is attuned to the temperature change.

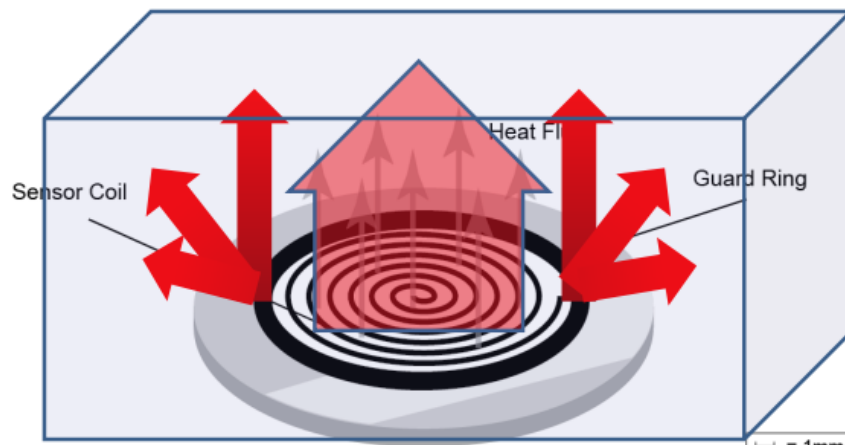


Figure 3.3: The sensor and guard ring demonstrating how heat is transferred in one directional plane to the sample [19]

Contact Agents

During testing of the material, it was critical to have very good contact between the sensor surface and test material to have accurate and repeatable measurements. The liquids such as the drilling fluids had a good contact with the sensor, but it was not the case with solids. Therefore, a contact agent was required for testing the solids. Two standard contact agents were offered with the C-Therm TCi system: Distilled Water and Wakefield 120 thermal grease. Contact agents have correction factors to prevent them from negatively affecting measurements. When the tests were run below 70°C the best contact agent was distilled water, as it has relatively high thermal conductivity ($\sim 0.6 \text{ W/mK}$), low viscosity, and is easy to apply and clean. When testing for long periods of time, or when testing porous or absorbent materials the Wakefield 120 thermal grease was used as the contact agent when testing at temperatures above 70°C. The limitation was how thick the layer of thermal grease had to be since excessively thick layer or sparingly applied layer affected the sensor readings.

Thermal Chamber

The C-Therm TCi is composed of a chamber workspace, control panel and machinery compartment. The C-Therm TCi has an operating range of -50 to 200 °C. Circulation of air is produced by a propeller type fan, which is driven by an externally mounted motor. The chamber is heated by recirculating chamber air through low-mass, open-air nichrome wire

heater elements in the conditioning plenum. The plenum is positioned in the chamber ceiling and is secluded from the workspace to prevent direct radiation of heat. The chamber is cooled by recirculating chamber air through a refrigerated cooling coil in the conditioning plenum. The Tenney Jr. thermal chamber with Watlow F4 controller is the thermal chamber supported by C-Therm for use with the TCi. When operating the TCi sensor in a thermal chamber, it is possible for some electrical leakage to pass from the thermal chamber floor through to the sensor which will adversely impact the accuracy of testing results and eventually damage the sensor if operated at elevated temperatures over long periods of time. Therefore, it is recommended to place a non-electrically conductive layer between the sensor base plate and the thermal chamber floor as shown in Figure 3.7. A silicone rubber is a perfect electrically insulative material for this purpose. It isolates the sensor from the thermal chamber and will prevent any potential electrical leakage.

High Pressure Cell

To mimic the pressure and temperature conditions downhole, C-Therm has provided a complementary Pressure Valve Assembly. This assembly consists of a Pressure cell, equalizing tube, Swagelok tubing, TCi sensor assembly, pressure relief valve set to 400 psi, pressure gauge and an On an Off valve as shown in Figure 3.4 which pressurizes the test material s if it were in a well. The High pressure cell was used in conjunction with the thermal chamber at varying temperature just like that of a wellbore.

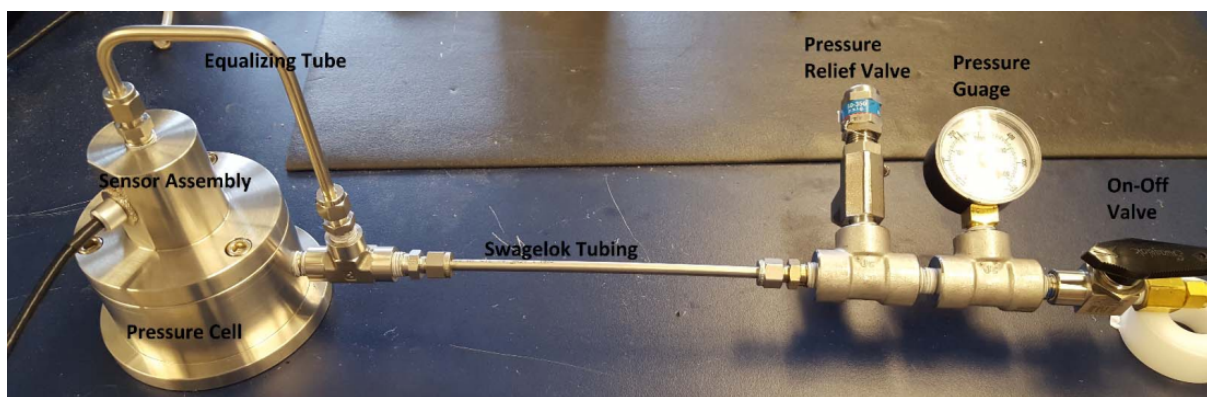


Figure 3.4 The high pressure cell assembly with the equalizing tube connecting the pressure relief valve, the pressure gauge and On-Off valve by a Swagelok tubing. (Testing with High Pressure Cell) [20]

3.3 Experimental procedure

An advantage of using the C-Therm TCi thermal conductivity analyzer is that samples to be tested requires no tedious preparation or any preparation at all.

3.3.1 Testing of Liquids

For liquids tested, the high pressure cell was employed. Samples required no contact agent. The samples were poured into the high pressure cell to the fill line level. The sensor is carefully lowered on it to prevent bubbles from forming in the fluid while making sure the O-ring is inserted into the O-ring groove and then placed into the thermal chamber. The fill line and O-ring is seen in the high pressure cell in figure 3.5.

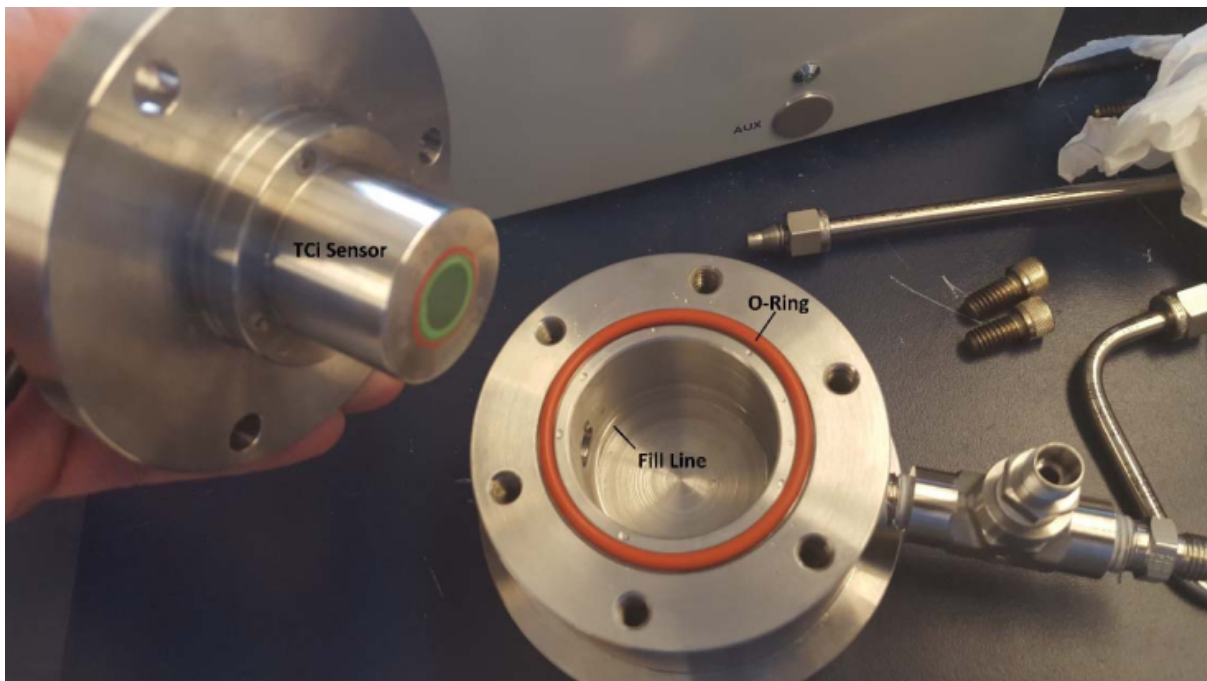


Figure 3.5 The high pressure cell for liquid tests showing the TCi sensor, fine line and O-ring. (Testing with High Pressure Cell) [20]

3.3.2 Testing of Solids

The solid material was placed on the TCi sensor with contact agent to establish good contact between the sample and sensor. Drops of distilled water or a thin layer of Wakefield 120 thermal grease was applied on the surface of the sensor depending the type of material and duration of test. Then, the sample is placed on the sensor inside the thermal chamber. Some sample which weighed less than 150 grams required additional weight to establish good contact

with the sensor. It was critical that, gloves were used to minimize heat transfer from your hands to the tested materials as high conductivity materials will quickly absorb heat from your hands, and will create a temperature gradient, which may affect the results. Another important consideration was that, the surface of the solid samples in contact with the sensor had to be smooth because, rough surfaces create an affective thick layer of contact agent and will add to the total error in readings. Specific temperature at various time range control were input into the software on the computer after which the thermal conductivity and effusivity were being recorded and displayed on the screen. The temperature and time controls can also be input manually into the control panel on the thermal chamber. After the test has been completed, the sensor had to be cleaned by a special solution and a soft paper/textile towel.

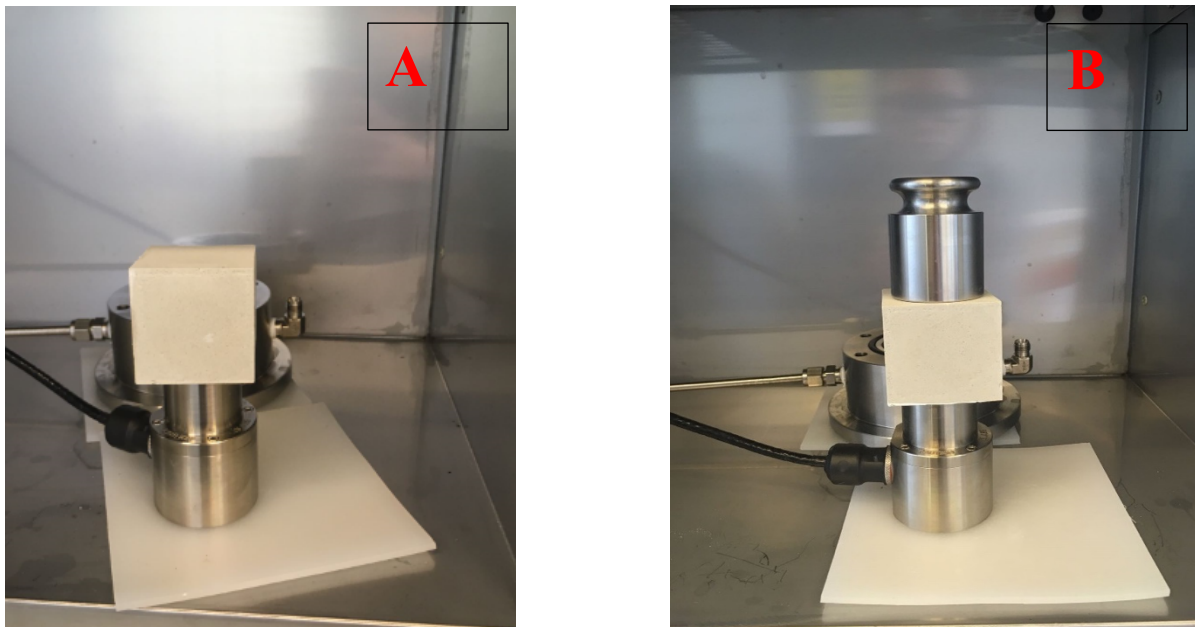


Figure 3.6 The sample positioned on sensor with no additional weight (A) and with additional weight (B) and a silicon rubber between the sensor base plate and the thermal chamber floor.

If the automatic control of the temperature is desired, a test method has to be configured beforehand. This is done by clicking an Add Control button on the main panel. The same temperature point has to be specified twice: once for ramping up and once for holding the constant temperature (soaking), see Figure 3.7. It was experimentally found, that for testing solids, much longer soak period is required for the specimen to come to thermal equilibrium. A summary of the general experimental procedure is shown in Figure 3.8.

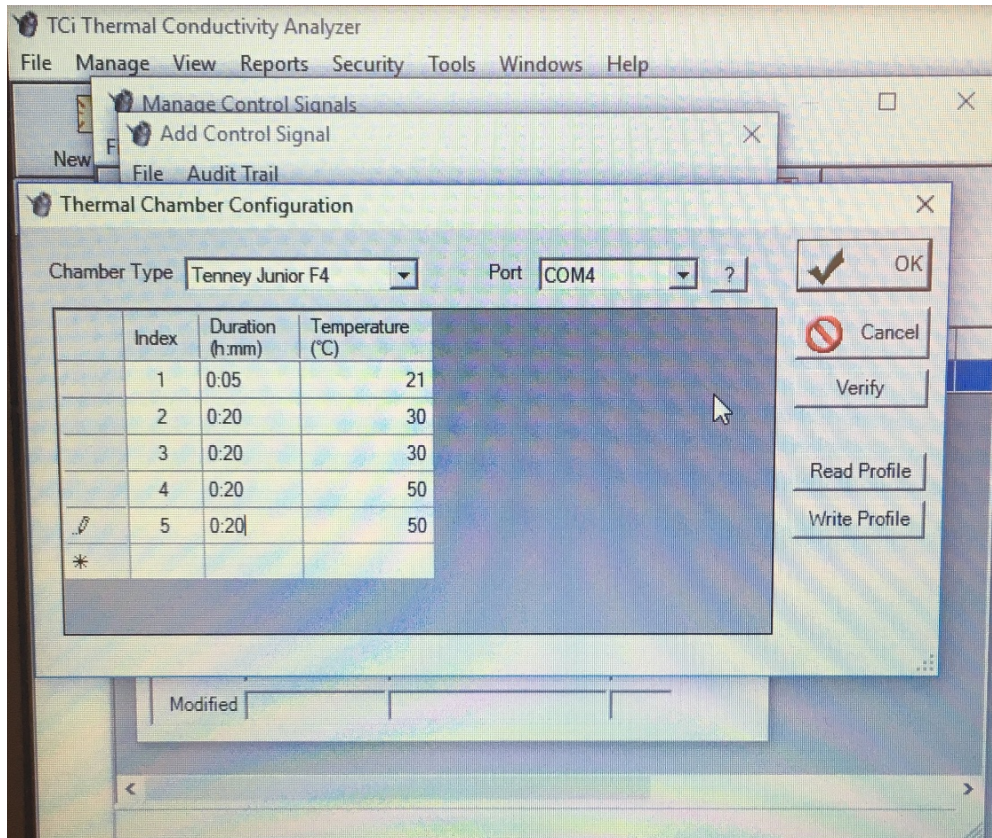


Figure 3.7: Thermal chamber configuration for automatic temperature control

Table 2: Summary of material type with their required thickness, preparation, temperature range and contact agent .

Material Type	Minimum Thickness	Power Level	Temperature Range (°C)	Sample Setup & Preparation	Contact Agent
Liquids	1 mm	37	-50 to 192	Use Small Volume Test Kit	None
Powders	1 mm	37	-50 to 192	Use Compression Test Accessory or Small Volume Test Kit	
Foams	2 mm	60	-50 to 192	Place sample on sensor. Place weight on sample.	
Fabrics	2 mm	37	-50 to 192	Use Compression Test Accessory	
Polymers	5 mm	37	-50 to 192	Place contact agent on sensor. Place sample on sensor. Place weight on sample.	5 to 70°C - 3 drops water 25 to 200°C - Wakefield 120 thermal grease*
Ceramics	5 mm	37	-50 to 192		
Low Metals (15 to 90 W/mK)	5-12 mm	65	-50 to 192		
High Metals (90 to 500 W/mK)	12-21 mm	65	-50 to 192		

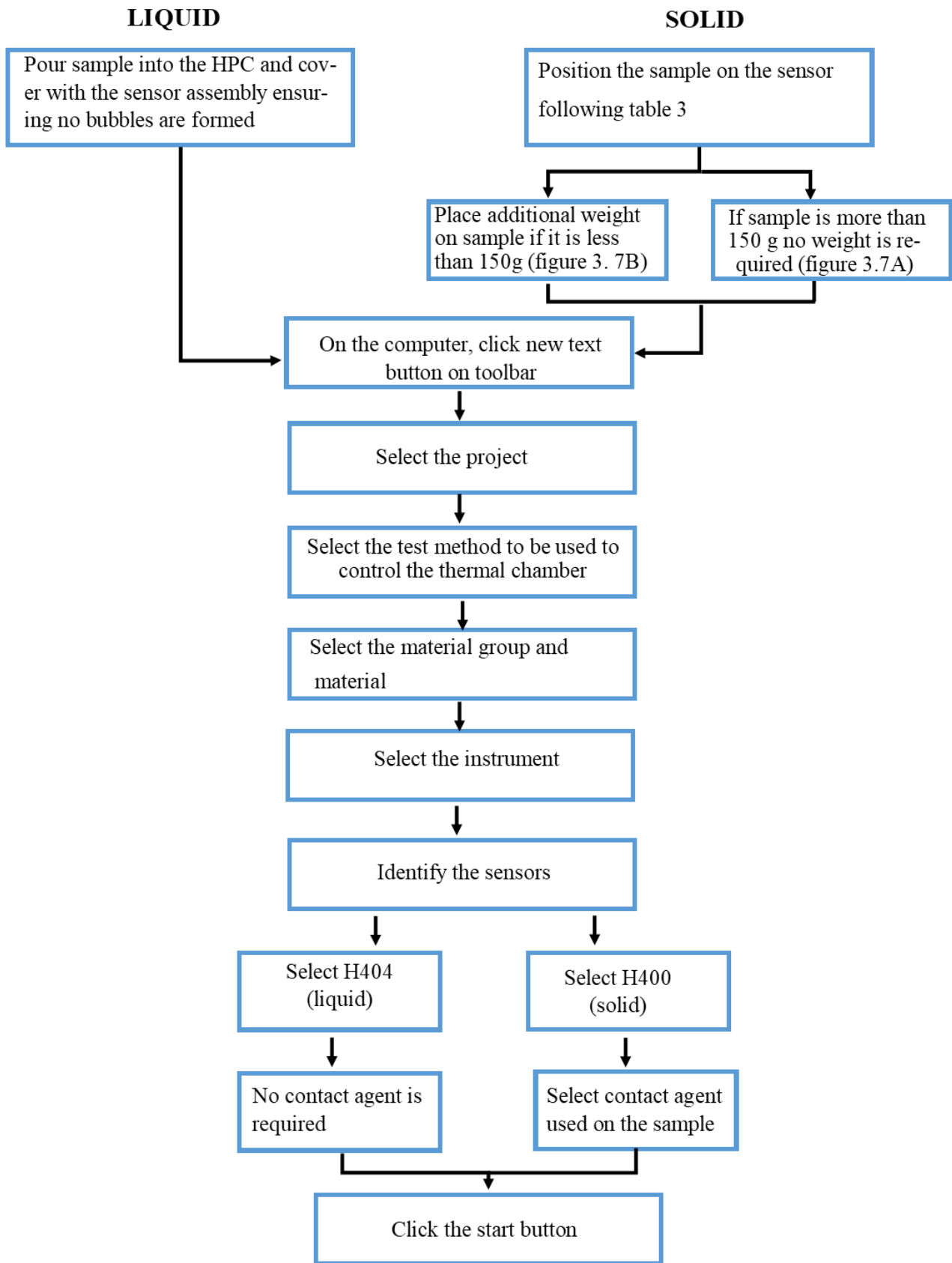


Figure 3.8: Experimental procedure

Chapter 4

4 Experimental Results and Regression Models

4.1 Introduction

In this chapter, findings from experiments performed to measure thermophysical properties of typical wellbore components are presented. The results are presented under four main subsections; cement properties, formation properties, fluid properties and casing properties. Linear and polynomial correlations of thermal conductivity of the materials are derived with temperature as the only variable. The knowledge of how these properties vary with temperature is of prime importance as they are present in heat transfer calculations. Neglecting the temperature dependence may lead to inaccurate calculations.

4.2 Cement Properties

The four polymers used include, G-Class, W50, Fly ash and Ground Granulated Blastfurnace Slag (GGBFS). Different correlations for thermal conductivities were developed from the different polymers, which are quite similar.

It was found that thermal conductivity decreases with temperature for all cement systems. The conductivities of GGBFS and W50 were quite similar. G-Class Cement had the highest thermal conductivity with Fly ash having the lowest. This observation was also made by Chokotaweekarn et al (2009) [21] who found from tests that the replacement of cement by fly ash resulted in lower thermal conductivity. This means that the Fly ash cement is applicable as a cementing material for geothermal wells, because it is able to prevent heat loss sufficiently, when hot water or steam is transported from the ground to the surface [21]. It also has good sealing properties that prevent influx. Cement composition was found to play an important role in the thermal conductivity values obtained for these cements.

Laboratory experiments by Won et al. (2016) [22] for G-class cement performed based on the mixture design proposed by Philippacopoulos and Berndt (2000) [23] revealed that thermal conductivity of G-Class Cement decreases with temperature increase (Table 3, Figure 4.1b).

The difference in range of values between the results of Won et al. (2016) [22] and our results could be due to the cement composition, cement system characteristics, experimental errors and prevailing conditions.

Table 3: Thermal conductivity of G-class cement specimen [22].

Temperature T (°C)	Thermal Conductivity k, (W/mk)
20	0.6798
50	0.6243
100	0.5

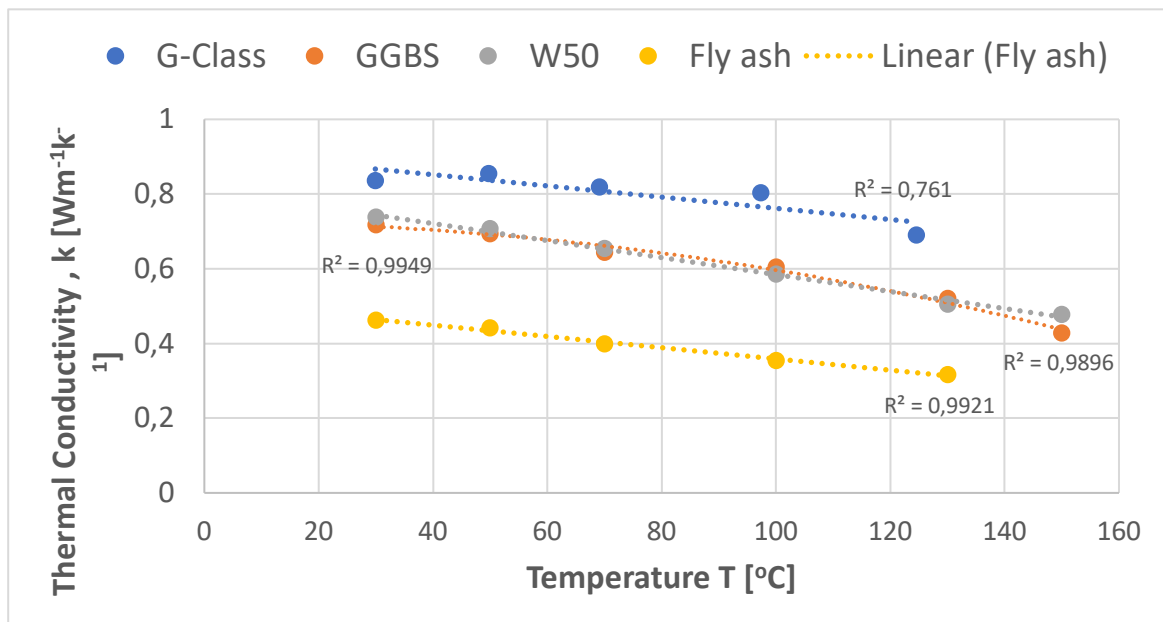


Figure 4.1a: Thermal Conductivity for cement polymers as a function of temperature

$$k_{cg} = -0.0015T + 0.9119 \quad \text{Eq. 4.1}$$

$$k_{W50} = -0.0023T + 0.8121 \quad \text{Eq. 4.2}$$

$$k_{GGBFS} = 1 \times 10^{-5}T^2 - 4 \times 10^{-5}T + 0.7254 \quad \text{Eq. 4.3}$$

$$k_{fa} = -0.0015T + 0.5093 \quad \text{Eq. 4.4}$$

Where; k_{cg} =Thermal conductivity of G-Class cement [W/mk]

k_{w50} = Thermal conductivity of W50 cement [W/mk]

k_{GGBS} = Thermal conductivity of GGBS cement [W/mk]

k_{fa} = Thermal conductivity for fly ash [W/mk]

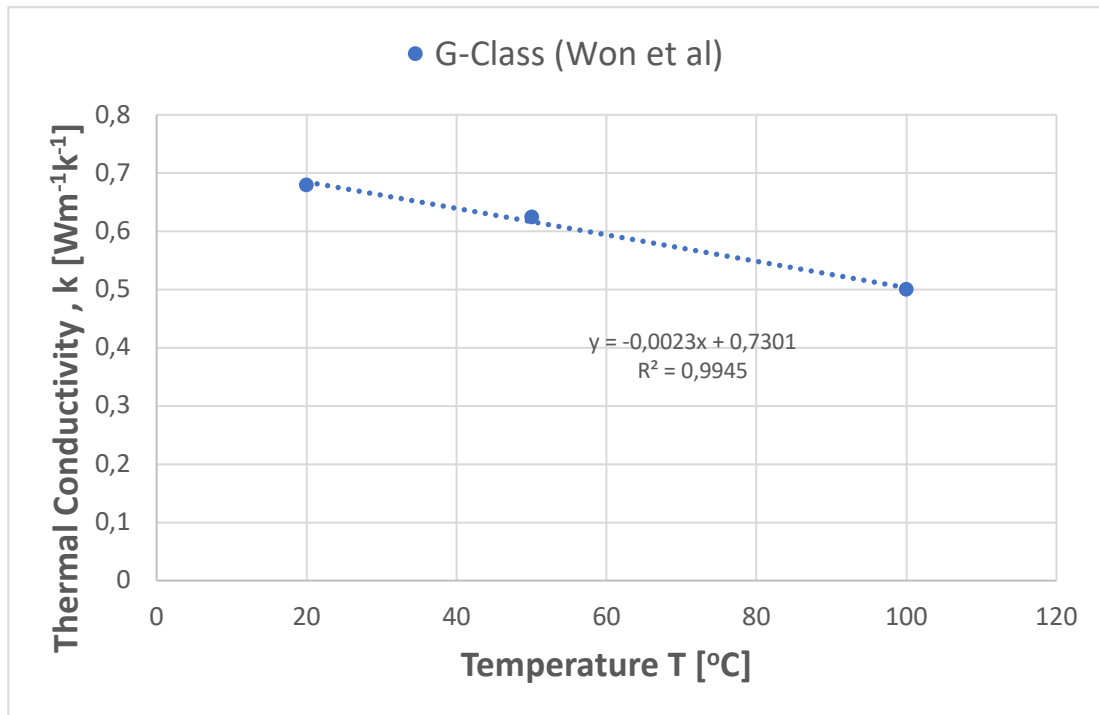


Figure 4.1b: Thermal Conductivity as a function of temperature (Won et al 2016) [22]

4.3 Casing Properties

Two types of metals were tested, Steel ST52 and Stainless Steel 316. Generally the thermal conductivity of the metals increased with temperature (Figure 4.2). The results of stainless steel 316 corroborated quite well with the experiments by Thermtest [24], a dealer in Thermophysical instruments. They performed thermal conductivity measurements at increasing temperatures (between 21°C-200 °C) on stainless steel 316 using the Hot Disk TPS 2200 thermal conductivity instrument. The thermal conductivity of the steel sample increased with increasing temperature over the entire temperature range studied as seen in Figure 4.3 They also tested other metals which showed similar trends in thermal conductivity as a function of temperature. Our results for Steel ST52 though not tested by Thermtest, can be inferred to be quite accurate since it follows a trend of similar tested metals.

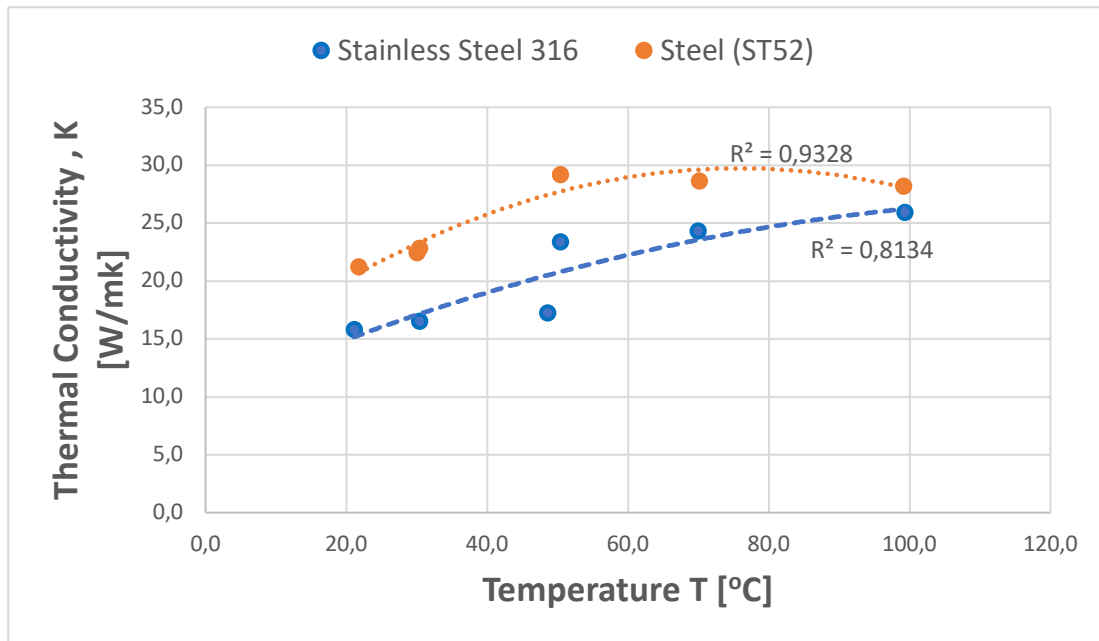


Figure 4.2 Thermal Conductivity as a function of temperature for Stainless Steel 316 and Steel ST52

$$K_{S316} = -0.001T^2 + 0.2655T + 10.034 \quad \text{Eq. 4.5}$$

$$K_{ST52} = -0.0031T^2 + 0.4688T + 11.951 \quad \text{Eq. 4.6}$$

Where:

K_{S316} = Thermal conductivity of Stainless Steel 316, [W/mk]

K_{ST52} = Thermal conductivity of Steel (ST52), [W/mk]

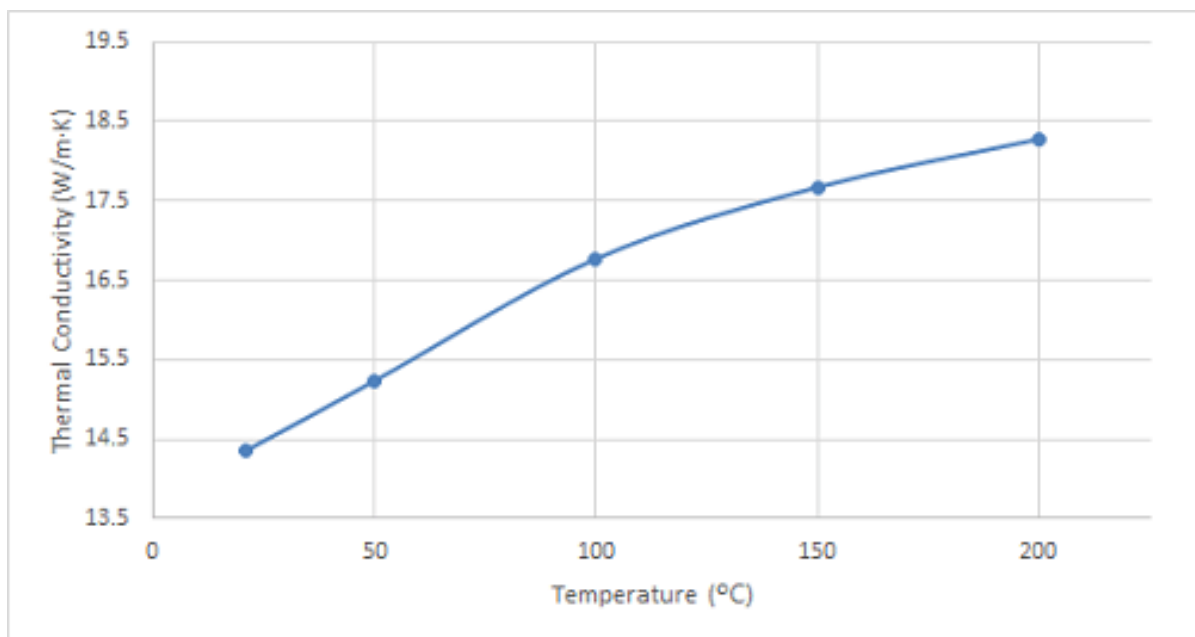


Figure 4.3 Thermal Conductivity as a function of temperature for Stainless Steel 316 [24]

4.4 Fluid Properties

For the fluids both produced fluids and annular fluids were tested. In this case, oil and distilled water are considered the produced fluid whiles brine and water based mud (WBM) are considered for annular fluids

4.4.1 Crude Oil

i. Thermal Conductivity

Liquids in general have lower thermal conductivities compared to solids and from Figure 4.4 we observe very low thermal conductivities for our results. The figure also shows a plot using a correlation for thermal conductivity as a function of temperature by Das et al. (2000) [25]. Our results agrees quite well with their results.

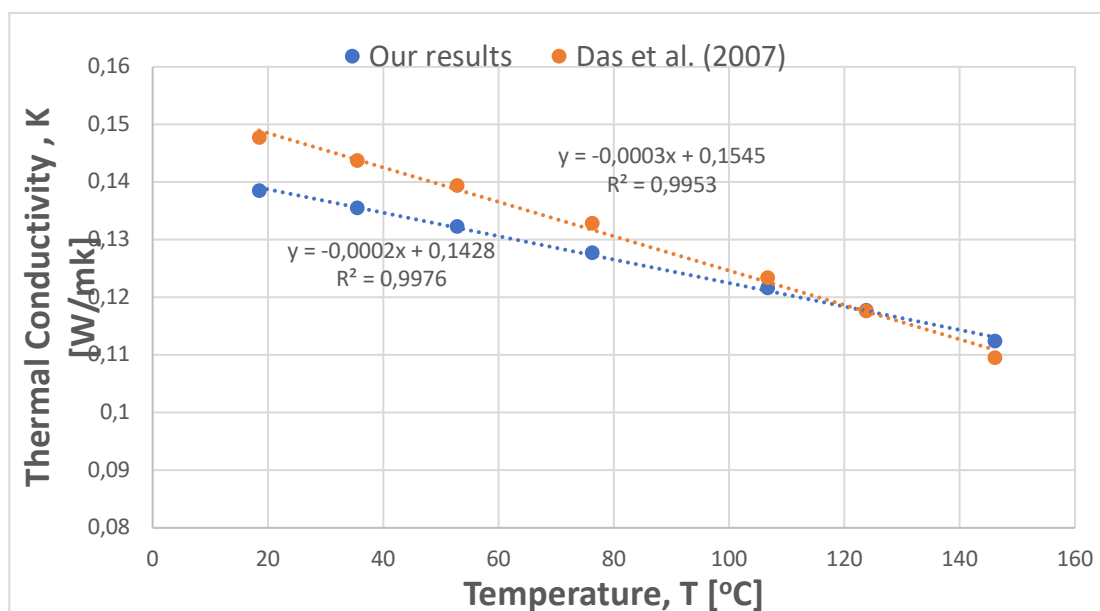


Figure 4.4 Thermal Conductivity as a function of temperature for oil

$$k_o = -0.0002T + 0.1428 \quad \text{Eq. 4.7}$$

$$k_{oD} = -0.0003T + 0.1545 \quad \text{Eq. 4.8}$$

Where:

k_o = Thermal conductivity of oil, [W/mk]

k_{oD} = Thermal conductivity of oil by Das et al. (2000) [25], [W/mk]

For density, viscosity and specific heat capacity, correlations and assumptions adopted by Horpestad (2017) [13] in his thesis work are used. This current work is a build up to the work by Horpestad so it is appropriate to adopt his correlations.

ii. Density

The density as a function of temperature and pressure may be described by the following equation of state (Standing's relationship, found in Sattarin, et al (2007) [26]):

$$\rho = \rho_{sc} + \Delta\rho_p - \Delta\rho_T \quad \text{Eq. 4.9}$$

$$\Delta\rho_p = [0.167 + 16.181 \times 10^{-0.0425\rho_{sc}}] \left(\frac{P}{1000} \right)$$

$$\Delta\rho_T = \left[0.0133 + 152.4(\rho_{sc} + \Delta\rho_p)^{2.45} \right] (T - 520) - [(8.1 \times 10^{-6} - 90.0622) \times 10^{0.764(\rho_{sc} + \Delta\rho_p)}] (T - 520)^2$$

Where:

ρ : Density of oil at pressure and temperature (lbm/ft³)

ρ_{sc} : Density at standard conditions (lbm/ft³)

$\Delta\rho_T$: Density correction for thermal expansion (lbm/ft³)

$\Delta\rho_p$:Density correction for compression (lbm/ft³)

T :Temperature (°R)

P :Pressure (psi)

iii. Specific Heat Capacity

We use the correlation by Wright (2014) [27]. This simple equation provide approximations for the variation of density and specific heat of crude oils of varying API gravity.

$$C_{p_o} = [(2 \times 10^3 T - 1.429)sg + 2.67 \times 10^3 T + 3.049] \times 10^3 \quad \text{Eq. 4.10}$$

where:

C_{p_o} :Specific heat capacity of dead oil at T [Jkg⁻¹ K⁻¹]

sg :Specific gravity of dead oil

iv. Viscosity

The dead oil viscosity as a function of temperature is given by the Beggs-Robinson correlation [28]:

$$\mu_{od} = 10^X - 1$$

Eq. 4.11

$$X = yT^{-1.163}$$

$$y = 10^Z$$

$$Z = 3.0324 - 0.02023\gamma_o$$

where: μ_{od} : Dead oil viscosity at T (cP) ; γ_o : Dead oil density (°API) ; T : Temperature (°F)

4.4.2 Water Based Mud (WBM)

This sample is composed of two mixtures, prepared separately and mixed together at the very end. The main mixture is in an aggregated state, which means that single particles are tied together in aggregates. The supplementary mixture is in a flocculated state, which means that there are net to attractive forces between single particles or aggregates. Particles or aggregates are bound together creating loose structures. The aggregated state is achieved by mixing water with salts and then adding bentonite, while the flocculated state is reached by mixing water and bentonite, and adding salts afterwards. The mud recipes are given in the tables below.

Table 4: Ingredients for the main mixture (WBM)

Water, pH 9.5	200 ml
NaCl	1 g
CaCl ₂ x2H ₂ O	1 g
Bentonite	12 g
Barite	20 g

Table 5: Ingredients for the supplementary mixture (WBM)

Water, pH 9.5	300 ml
Bentonite	30 g
NaCl	1.6 g
CaCl ₂ x2H ₂ O	1.6 g
Ca(OH) ₂	0.8 g
MgSO ₄ x7H ₂ O	0.2 g

i. Thermal Conductivity

The plot in Figure 4.5 shows an increasing thermal conductivity with temperature increase.

$$k_{WBM} = 0.0106T + 0.3041 \quad \text{Eq. 4.12}$$

Where:

K_{WBM} = Thermal conductivity of water based mud [W/mK]

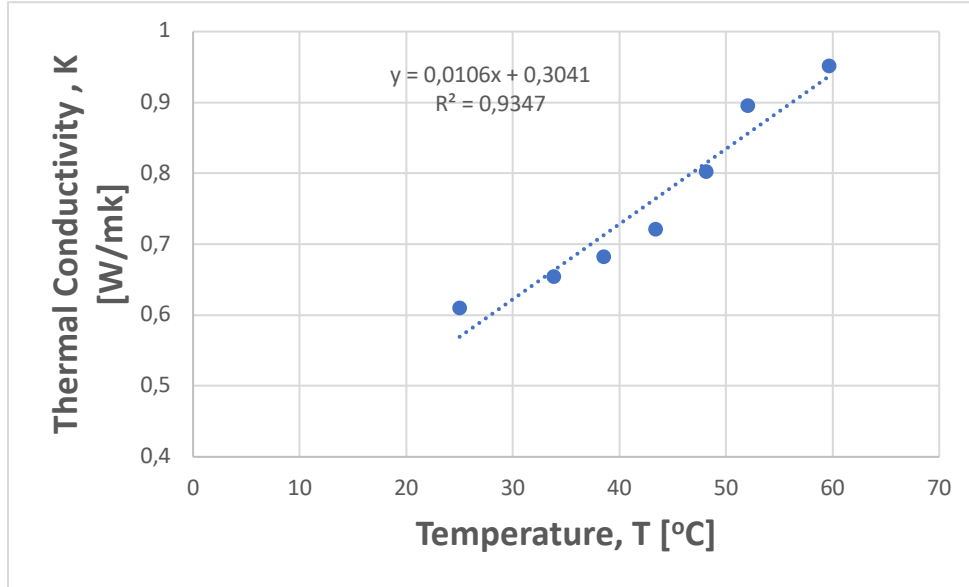


Figure 4.5 Thermal Conductivity as a function of temperature for WBM

ii. Density

To predict the density of the water base mud, we use the empirical equation of Zheng et al (2017) [29] which relates mud density and temperature.

$$\rho_{WBM} = \rho_{mo} [1 + \gamma_T(T - T_o) + \gamma_{TT}(T - T_o)^2] \quad \text{Eq. 4.13}$$

$$\begin{aligned} \gamma_T &= -4.536 \times 10^{-4} \\ \gamma_{TT} &= -1.972 \times 10^{-6} \\ \rho_{mo} &= 1014 \frac{kg}{m^3} \end{aligned}$$

Where, ρ_{WBM} is mud density

ρ_{mo} is initial mud density at standard conditions,

T_o is initial temperature at standard condition. [K]

γ_T and γ_{TT} , are empirical constants.

iii. Specific Heat Capacity

Heat capacity can be written as a function of thermal conductivity, thermal effusivity and density.

$$C_p = \frac{\epsilon^2}{k * \rho} \quad \text{Eq. 4.14}$$

Where C_p = Specific heat capacity, [$\text{Jkg}^{-1} \text{K}^{-1}$]

ϵ = thermal effusivity

ρ = density (Density was calculated as a linear function of temperature) [kg/m^3]

Using our experimental data (ϵ, k) to fit into equation 4.13, we arrived at the polynomial equation below, which is an equation with temperature as a variable. The plot is shown on Figure 4.6

$$C_{pWMB} = -0.0104T^3 + 1.2674T^2 - 36.832T + 3995.9 \quad \text{Eq. 4.15}$$

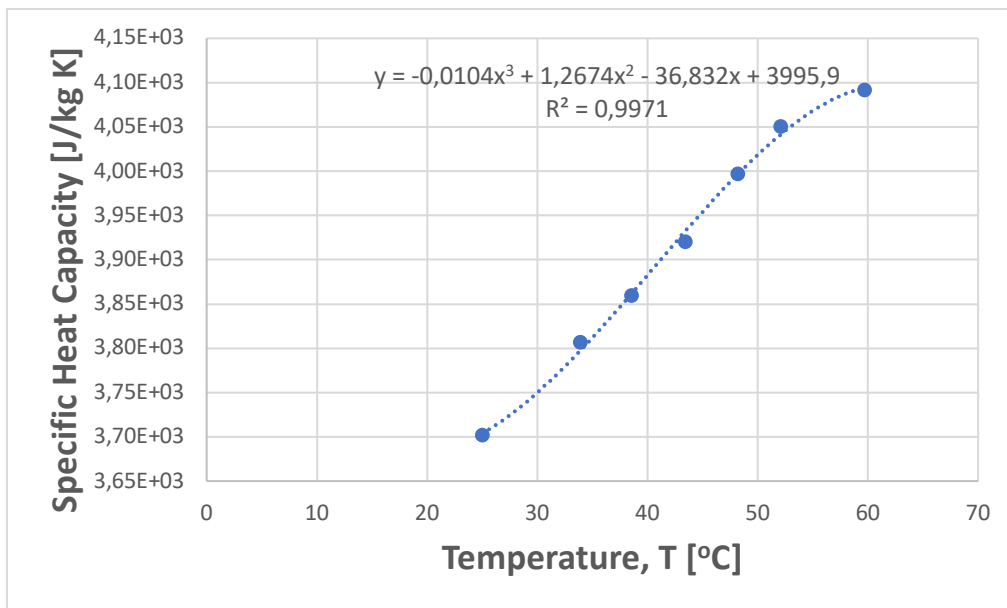


Figure 4.6 Specific heat capacity as a function of temperature for WBM

iv. Viscosity

We adopt here a correlation by Santoyo et al (2001) [30] for viscosity of non-Newtonian water based mud as a function of temperature for high temperature drilling mud systems (HTDFS). This model remains valid for a wide range of temperature and as such is most appropriate to use here. Also the measurements are in SI units which follows correctly the units of the preceding models. Figure 4.7 shows a plot of viscosity verses temperature for the mud system

and a comparison to water. Normally viscosity will reduce with temperature and we observe that on the figure.

$$\mu_m = 15.7688 - 0.04205776T - 8.038 \times 10^{-5}T^2 \quad \text{Eq. 4.16}$$

Where: μ_m = viscosity of water based mud [cP]

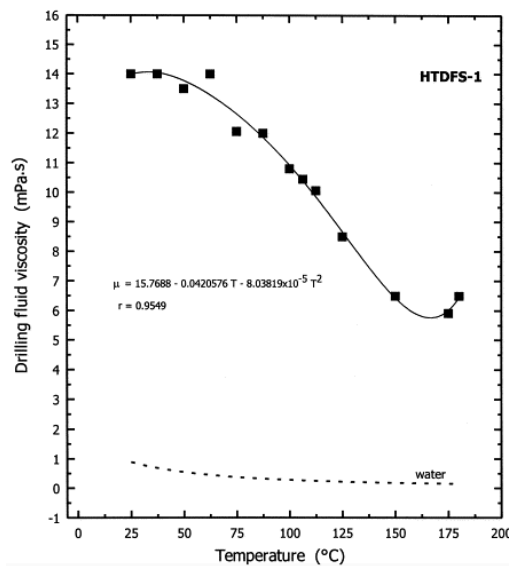


Figure 4.7: Variation in viscosity with temperature for drilling fluid (WBM) [30]

4.4.3 Distilled Water

i. Thermal Conductivity

Figure 4.8 shows our experimental results for thermal conductivity of distilled water and that of Ramires et al (1995) [31]. The observed difference could be from prevailing pressures and temperatures at which results were taken or due to different instrument calibrations. The most important thing here the general increase in thermal conductivity of water with temperature.

Our correlation therefore is:

$$k_w = 0.0008T + 0.5155 \quad \text{Eq. 4.17}$$

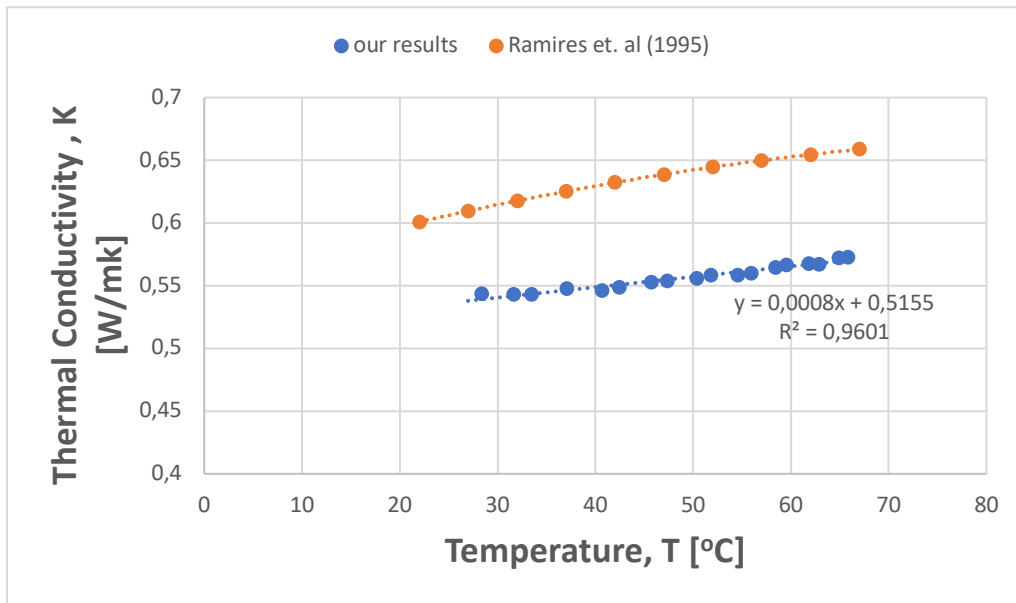


Figure 4.8: Thermal conductivity of distilled water

ii. Density

The density of water decreases with temperature increase as seen in Figure 4.9. This makes sense because, as heat is added to the liquid water, there is greater kinetic energy of the molecules and there are also more vibrations of the water molecules. Together, this mean that each water unit in liquid takes up more space as the temperature increases.

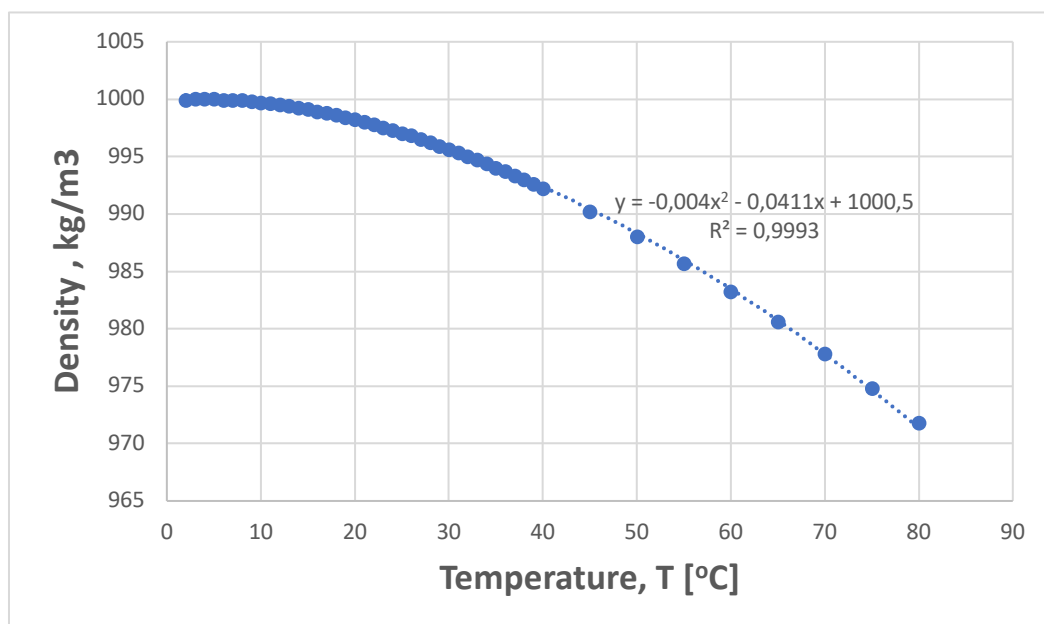


Figure 4.9: Density of distilled water with temperature [32]

The correlation of the above curve taken from IAPWS (2008) [32] is used in this work.

$$\rho_w = -0.004T^2 - 0.0411T + 1000.5 \quad \text{Eq. 4.18}$$

iii. Specific Heat Capacity

The specific heat capacity of distilled water was estimated using Equation 4.14. and the temperature dependent density was calculated with Equation 4.18.

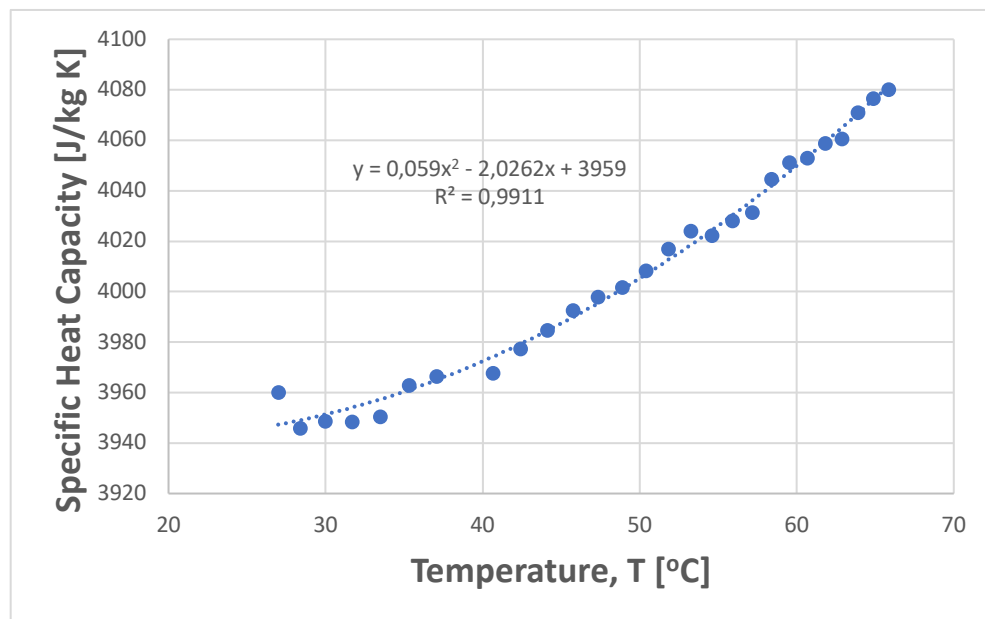


Figure 4.10: Specific heat capacity of distilled water

Figure 4.10 shows the variation of specific heat capacity with temperature. The accompanying correlation is;

$$Cp_w = 0.059T^2 - 2.0262T + 3959 \quad \text{Eq. 4.19}$$

Where: Cp_w = specific heat capacity of distilled water, [$\text{Jkg}^{-1} \text{K}^{-1}$]

iv. Viscosity

Here we plot viscosity against temperature using dynamic viscosity values provided by the International Association for the Properties of Water and Steam, IAPWS (2008) [32] in order to generate a temperature dependent viscosity correlation

$$\mu_w = 0.0003T^2 - 0,0365T + 1659 \quad \text{Eq. 4.20}$$

Where μ_w = Viscosity of distilled water [cP]

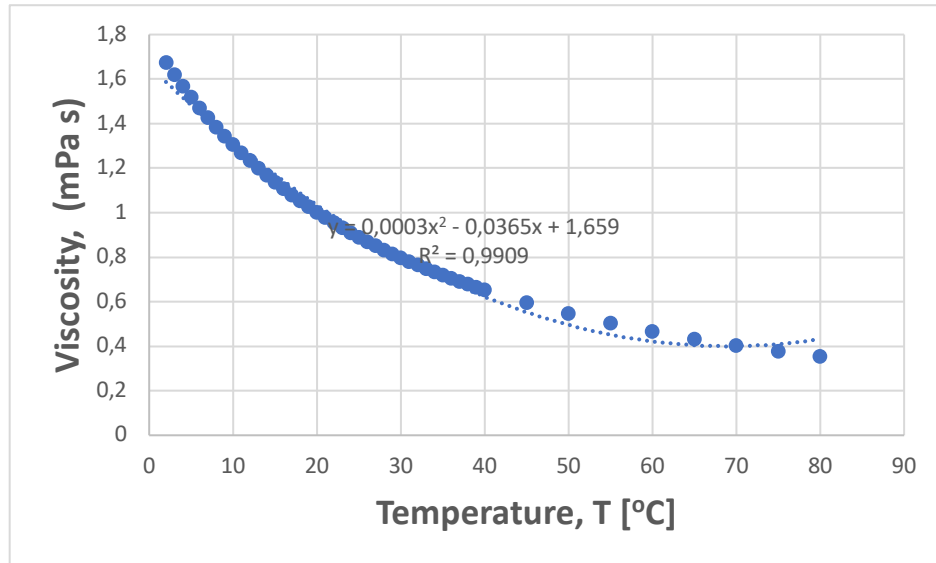


Figure 4.11: Dynamic viscosity of distilled water

4.4.4 Salt Water

i. Thermal Conductivity

Synthetic sea water, NaCl solution (3.5% dissolved salt by weight) was prepared and tested at 1atm pressure. Thermal conductivity results got from the test is plotted in Figure B1 in Appendix B. The results show a deviation from the normal trend observed by other authors in their experiments. Sharqawy et al (2010) [33] compared the results of a number of authors in Figure 4.12. For the purposes of calculations, we will use a correlation we came up with using experimental data by Nayar et al. (2016) [34]. A plot of the data is shown in 4.13.

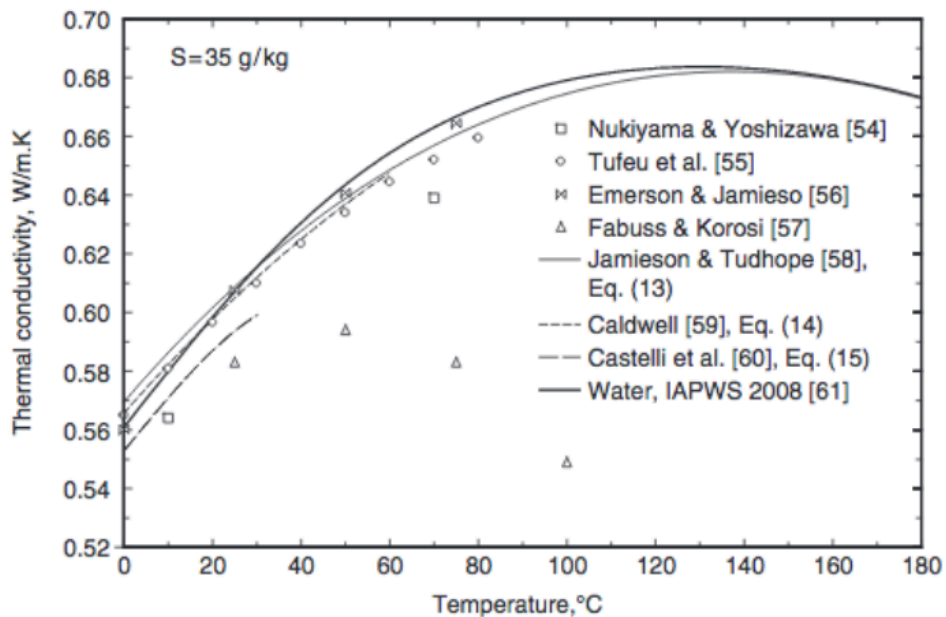


Figure 4.12: Seawater thermal conductivity vs. temperature (35g/kg) [33]

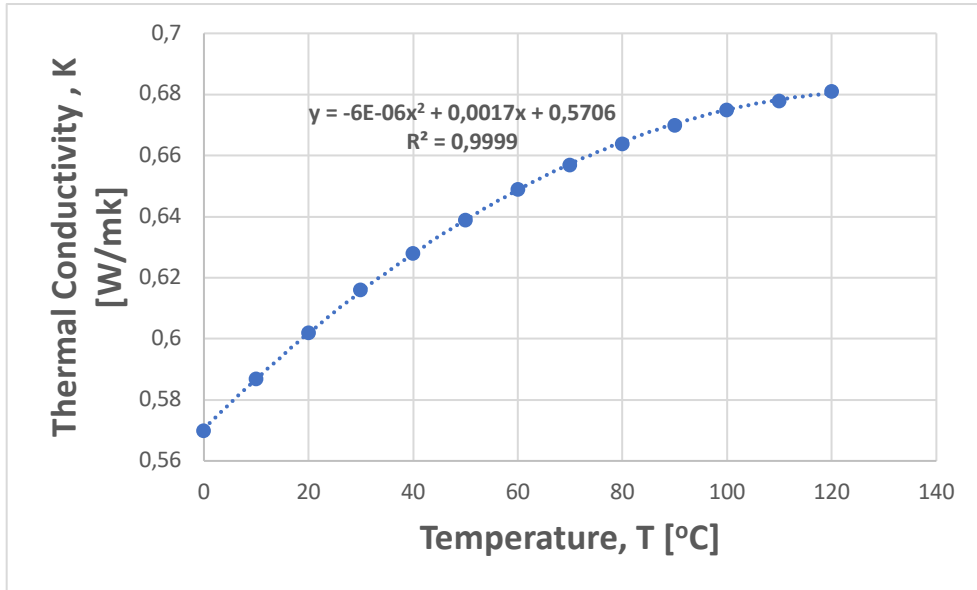


Figure 4.13: Thermal Conductivity of salt water (salinity =30g/kg) [34]

$$k_{sw} = -6 \times 10^{-6}T^2 - 0.0017T + 0.5706 \quad \text{Eq. 4.21}$$

Where k_{sw} = thermal conductivity of salt water [W/mK]

ii. Density

Nayar et al. (2016) [34] presented data for density of seawater with salinity of 35g/kg at a pressure of 1 atm. Since we made our testing at 1 atm pressure and 35g/kg, we plot their data in Figure 4.14 and generate a polynomial correlation to describe the relationship between density and temperature of seawater at constant salinity and pressure.

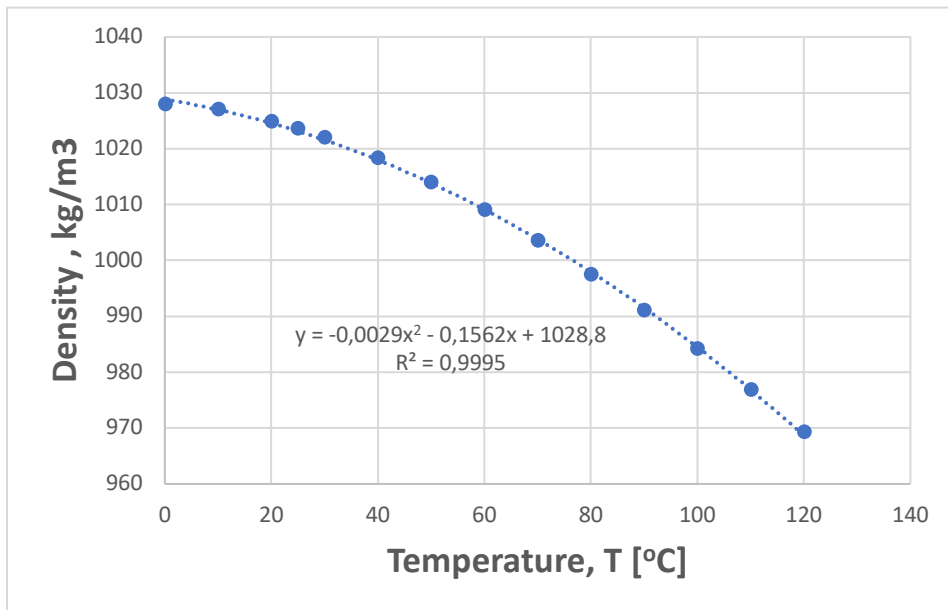


Figure 4.14: Density of salt water (salinity =35g/kg, P= 1atm) [34]

$$\rho_{sw} = 0.0029T^2 - 0.1562T + 1028.8 \quad \text{Eq. 4.22}$$

iii. Specific Heat Capacity

We plot data from Nayar et al (2016) [34], to generate the polynomial relation below

$$Cp_{sw} = 0.0043T^2 - 0.0874T + 3993.9 \quad \text{Eq. 4.23}$$

Where: Cp_{sw} = Specific Heat Capacity of salt water, [$\text{Jkg}^{-1} \text{K}^{-1}$]

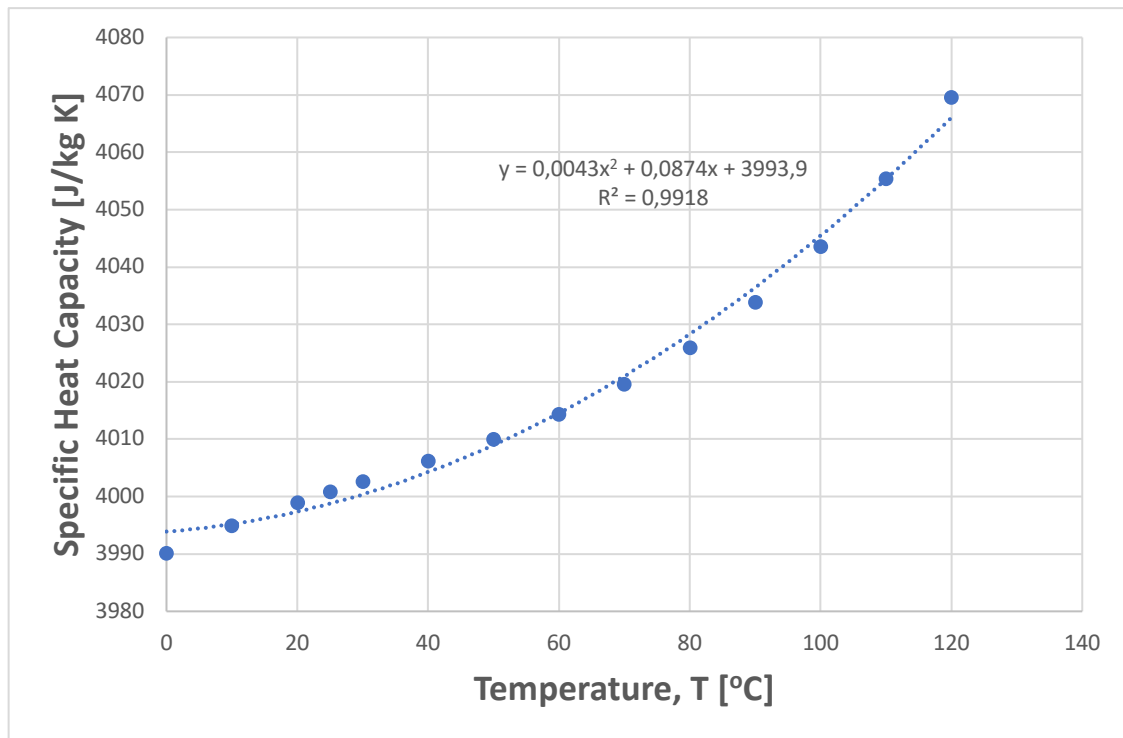


Figure 4.15 Specific heat capacity of salt water (salinity =35g/kg, P= 1atm) [34]

iv. Viscosity

The correlation is also generated from data provided by Nayar et al. (2016) [34].

$$Cp_{sw} = -2 \times 10^{-6}T^3 + 0.0005T^2 - 0.0465T + 1.8555 \quad \text{Eq. 4.24}$$

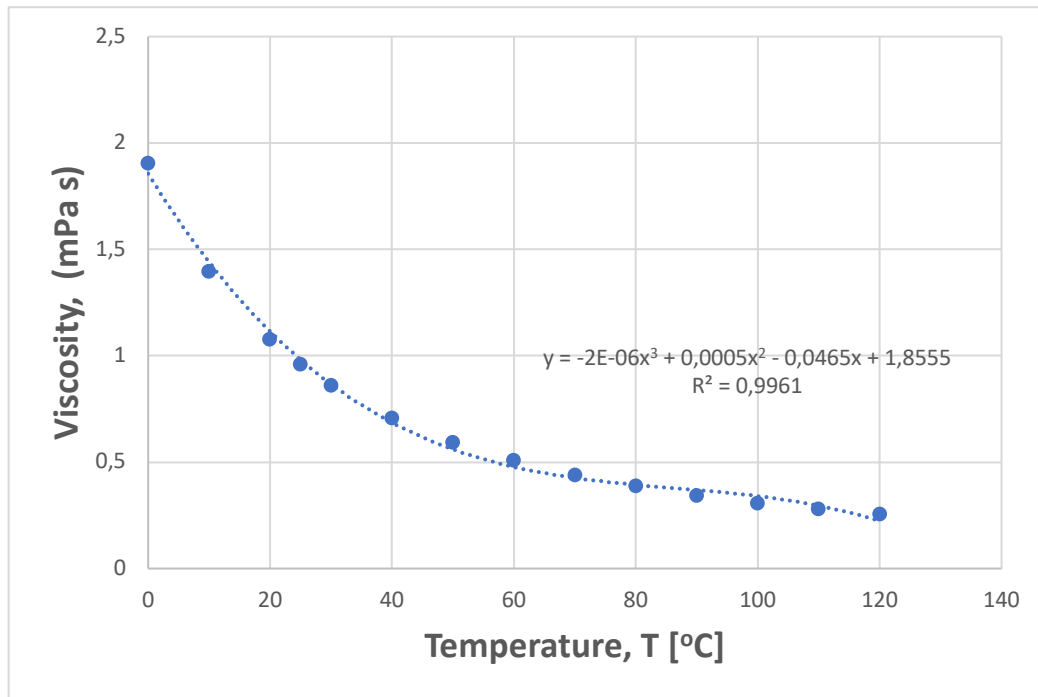


Figure 4.16 Viscosity of salt water (salinity =35g/kg, P= 1atm) [34]

4.5 Formation Properties

Three formation types were tested, namely Berea Sandstone, Bentheimer Sandstone, and Chalk. Berea generally has a higher porosity and permeability than Bentheimer. The choice of formation types is to test for both sandstones and carbonate rocks. The influence of fluids in the pores on conductivity is large as such dry rock samples were tested. It is assumed they were air saturated. We see from Figure 4.17 that thermal conductivity is very low for high porosity. Chalk has a higher porosity than Berea and Bentheimer, in that order. Thermal conductivities of dry rocks have been shown to be functions of density, porosity, grain size and shape, degree of cementation, and mineral composition. However, the effect of these properties were not considered in this work. Knowledge on these properties will undoubtedly help in explaining better the nature of the curves in Figure 4.17.

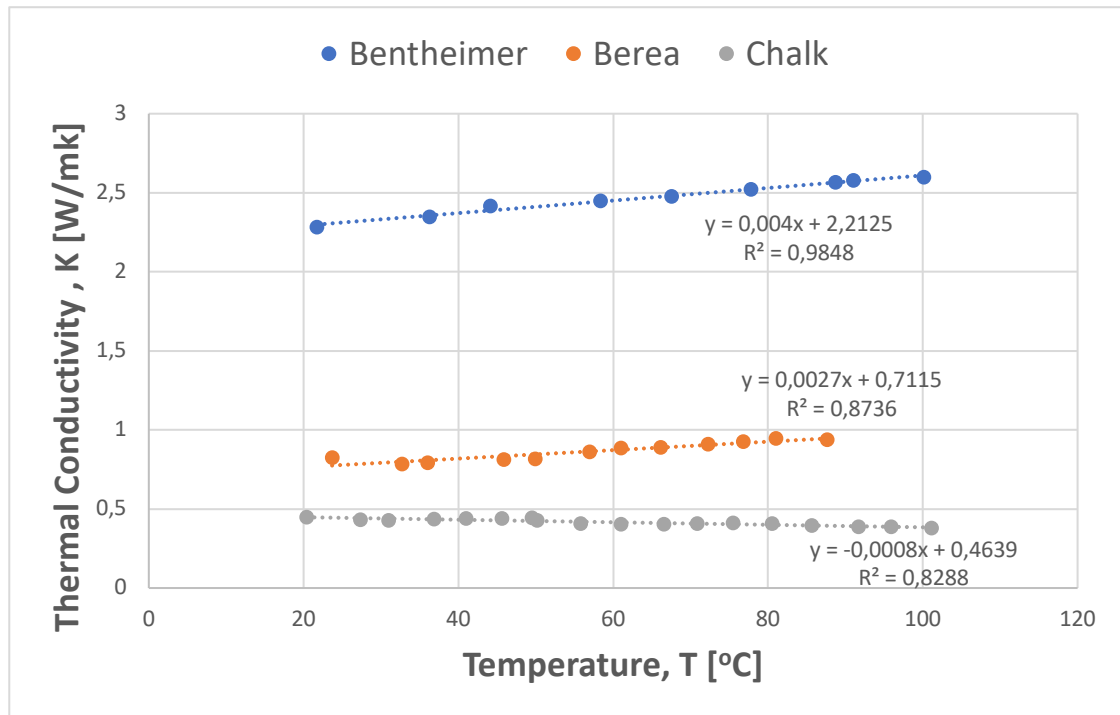


Figure 4.17: Thermal conductivity of formation types

The following correlations are developed to describe the thermal conductivity for the various rock types.

$$K_{Bent} = 0.004T + 2.2125 \quad \text{Eq. 4.25}$$

$$K_{Ber} = 0.0027T + 0.7115 \quad \text{Eq. 4.26}$$

$$K_{ch} = -0.0008T + 0.4639 \quad \text{Eq. 4.27}$$

Where; k_{Bent} = Thermal conductivity of Bentheimer, [W/mK]

k_{Ber} = Thermal conductivity of Berea, [W/mK]

k_{ch} = Thermal conductivity of Chalk, [W/mK]

Chapter 5

5 Well Configuration and Temperature Model

5.1 Introduction

This chapter presents the temperature model used in this work and the well configuration with all barriers considered. Also the model parameters for simulation the production scenario are presented.

5.2 Temperature Model

The temperature model used in this work was one used by Horpestad (2017) [13] which follows the model of Hassan and Kabir and Wang [1]. The model considers a hot reservoir fluid produced and single phase, rising up along the tubing. The produced fluid is assumed to be hotter than the temperature across the annulus, casing, cement and formation at all depths except at the bottom point of the well. The fluid therefore transports heat, $Q(z)$, into a control volume at z , and heat out of the control volume, $Q(z-\Delta z)$, at distance $z-dz$. The difference in heat in and out of the control volume must be equal to the amount of heat transferred to the formation. The model for fluid temperature at any point along the production tubing is expressed below; Details on the stepwise derivation of the model is attached in Appendix A.

$$T_{f(i)} = T_{ei(i)+A_d(i)} \left[1 - e^{-\frac{dz}{A_d(i)}} \right] \left(gG \cos\theta(i) + \phi(i) - \frac{g \cos\theta(i)}{C_{p1(i)}} \right) + e^{-\frac{dz}{A_d(i)}} (T_{f(i-1)} - T_{ei(i-1)}) \quad \text{Eq. 5.1}$$

Where: T_f = Fluid temperature, [K]

T_{ei} = Earth temperature, [K]

A_d = Relaxation distance [m]

dz = Control volume, [m]

gG = Geothermal gradient, [$^{\circ}$ K/m]

g = acceleration due to gravity, [m/s]

θ = inclination [deg]

The calculation procedure is a bottom up approach, thus from the bottom hole to the wellhead. Each subsequent calculation step is based on the fluid temperature of the former step as a boundary condition. For the first Cell, the temperature of the produced fluid (T_f) is assumed to be equal to the in-situ formation temperature (T_{ei}). $T_f = T_{bh} = T_{ei}$.

T_{bh} = bottomhole temperature.

5.2.1 Well Configuration

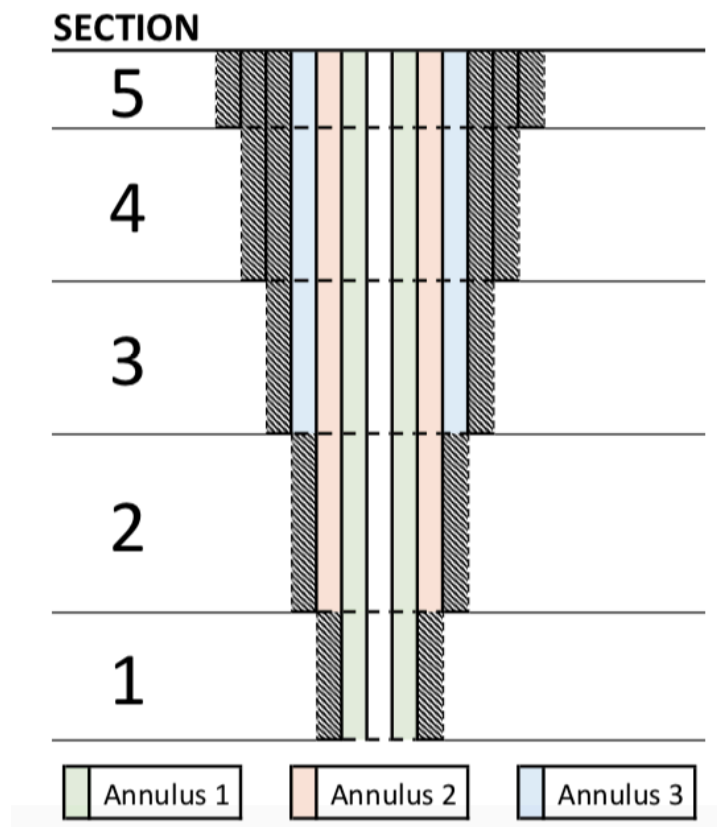


Figure 5.1: Well configuration [13]

The well consists of 5 casings and one production tubing. The casing strings are numbered from 1 to 5, with 1 being the deepest set casing. All the casing strings are suspended within the wellhead and cemented at least up to the previous casing shoe. Pressure build-up in annulus is not considered and any changes in well configuration dimensions due to temperature changes are not considered. Natural or free convection is considered to take place in the three fluid filled annulus, if the temperature conditions allow for such conditions are to arise.

The well is divided into five sections, where each section has a different configuration such as an additional casing, cement, etc. To calculate the Overall Heat Transfer Coefficient (U), for the entire well, U_{ti} have to be defined for each section.

The casing/tubing and wellbore dimensions, and the setting depths of casings are shown in Table 6

Table 6: Wellbore and casing/tubing dimensions for the well

Section	Hole size	Casing	Depth (m)
5	0.9144 m (36 in)	OD: 0.7620 m (30 in) ID: 0.7112 m (28 in)	200
4	0.6604 m (30 in)	OD: 0.5080 m (20 in) ID: 0.4826 m (19 in)	800m
3	0.4445 m (17 1/2 in)	OD: 0.3397 m (13.375 in) ID: 0.3093 m (12.175 in)	1400m
2	0.3111 m (12 1/4 in)	OD: 0.2445 m (9.625 in) ID: 0.2168 m (8.545 in)	2600m
1	0.2168 m (8 1/2 in)	OD: 0.1937 m (7.625 in) ID: 0.1619 m (6.375 in) Tubing: OD: 0.1397 m (5.500 in) ID: 0.1186 m (4.670 in)	3000m

5.2.2 Calculation of the Overall Heat Transfer Coefficient for the Different Well Sections

For the calculations to follow, the following parameters are used in the definitions of U_{ti} for each section

Table 7: Description of parameters used in the definition on U_{ti}

Parameter	Description [units]
h_{ti}	Tubing CHTC [$W m^{-2} K^{-1}$]
k_{tbg}	Thermal conductivity of the tubing [$W m^{-1} K^{-1}$]
$h_{ca(1,2,3)}$	Annulus 1, 2 and 3 natural CHTC [$W m^{-2} K^{-1}$]
$k_{csg(1,2,3,4,5)}$	Thermal conductivity of the casing [$W m^{-1} K^{-1}$]
$k_{cem(1,2,3,4,5)}$	Cement layer thermal conductivity [$W m^{-1} K^{-1}$]
r_{ti}	Tubing wall inside radius [m]
r_{to}	Tubing wall outside radius [m]
$r_{ci(1,2,3,4,5)}$	Casing wall inside radius [m]
$r_{co(1,2,3,4,5)}$	Casing wall outside radius [m]
$r_{wb(1,2,3,4,5)}$	Wellbore wall radius [m]
1,2,3,4,5	Subscripts for element representing its position in the wellbore
CHTC	Convective Heat Transfer Coefficient

5.2.2.1 Section 1 (casing shoe 1 to casing shoe 2)

Section 1 consist of the following resistances, left to right:

- i. The thin stagnant fluid film on the inside of the production tubing
- ii. The tubing wall
- iii. The fluid in annulus 1
- iv. The casing 1 wall
- v. The cement 1 sheath

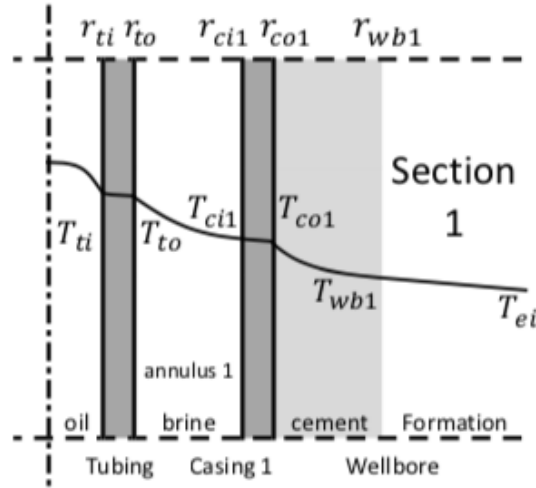


Figure 5.2: Temperature distribution throughout the wellbore cross section for section 1 [13]

$$R_{total1} = \frac{1}{2\pi r_{ti} L h_{ti}} + \frac{\ln\left(\frac{r_{to}}{r_{ti}}\right)}{2\pi L k_{tbg}} + \frac{1}{2\pi r_{ti} L h_{ca1}} + \frac{\ln\left(\frac{r_{co}}{r_{ci1}}\right)}{2\pi L k_{csg1}} + \frac{\ln\left(\frac{r_{wb1}}{r_{co1}}\right)}{2\pi L k_{cem1}} \quad \text{Eq. 5.2}$$

$$U_{ti1} = \frac{1}{R_{total1} A_{ti}}$$

$$U_{ti1} = \left[\frac{1}{h_{ti}} + \frac{r_{ti} \ln\left(\frac{r_{to}}{r_{ti}}\right)}{k_{tbg}} + \frac{r_{ti}}{r_{to} h_{ca1}} + \frac{r_{ti} \ln\left(\frac{r_{co}}{r_{ci1}}\right)}{k_{csg1}} + \frac{r_{ti} \ln\left(\frac{r_{wb1}}{r_{co1}}\right)}{k_{cem1}} \right]^{-1} \quad \text{Eq. 5.3}$$

5.2.2.2 Section 2 (casing shoe 2 to casing shoe 3)

Section 2 consist of the following resistances, left to right:

- i. The thin stagnant fluid film on the inside of the production tubing
- ii. The tubing wall
- iii. The fluid in annulus 1
- iv. The casing 1 wall
- v. The fluid in annulus 2
- vi. The casing 2 wall
- vii. The cement 2 sheath

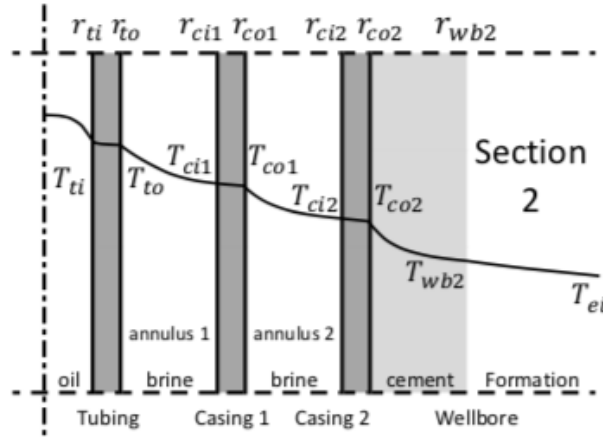


Figure 5.3: Temperature distribution throughout the wellbore cross section for section 2 [13]

$$R_{total2} = \frac{1}{2\pi r_{ti} L h_{ti}} + \frac{\ln\left(\frac{r_{to}}{r_{ti}}\right)}{2\pi L k_{tbg}} + \frac{1}{2\pi r_{to} L h_{ca1}} + \frac{\ln\left(\frac{r_{co1}}{r_{ci1}}\right)}{2\pi L k_{csg1}} + \frac{1}{2\pi r_{co1} L h_{ca2}} + \frac{\ln\left(\frac{r_{co2}}{r_{ci2}}\right)}{2\pi L k_{csg2}} + \frac{\ln\left(\frac{r_{wb2}}{r_{co2}}\right)}{2\pi L k_{cem2}} \quad \text{Eq. 5.4}$$

$$U_{ti2} = \frac{1}{R_{total2} A_{ti}}$$

$$R_{total2} = \left[\frac{1}{h_{ti}} + \frac{\ln\left(\frac{r_{to}}{r_{ti}}\right)}{k_{tbg}} + \frac{r_{ti}}{r_{to} h_{ca1}} + \frac{r_{ti} \ln\left(\frac{r_{co}}{r_{ci1}}\right)}{k_{csg1}} + \frac{r_{ti}}{r_{co1} h_{ca2}} + \frac{r_{ti} \ln\left(\frac{r_{co2}}{r_{ci2}}\right)}{k_{csg2}} + \frac{r_{ti} \ln\left(\frac{r_{wb2}}{r_{co2}}\right)}{k_{cem2}} \right]^{-1} \quad \text{Eq. 5.5}$$

5.2.2.3 Section 3 (casing shoe 3 to casing shoe 4)

Section 3 consist of the following resistances, left to right:

- i. The thin stagnant fluid film on the inside of the production tubing
- ii. The tubing wall
- iii. The fluid in annulus 1
- iv. The casing 1 wall
- v. The fluid in annulus 2
- vi. The casing 2 wall
- vii. The fluid in annulus 3
- viii. The casing 3 wall
- ix. The cement 3 sheath

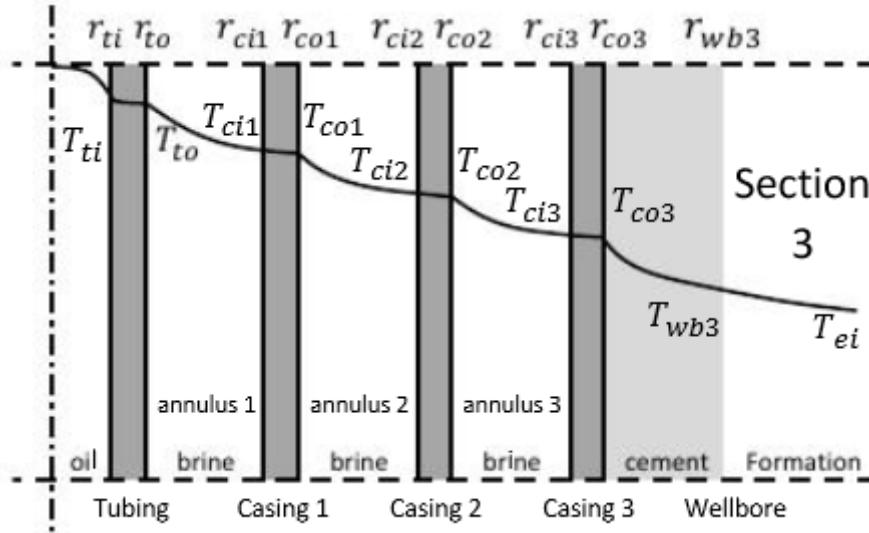


Figure 5.4: Temperature distribution throughout the wellbore cross section for section 3 [13]

$$R_{total3} = \frac{1}{2\pi r_{ti} L h_{ti}} + \frac{\ln\left(\frac{r_{to}}{r_{ti}}\right)}{2\pi L k_{tbg}} + \frac{1}{2\pi r_{to} L h_{ca1}} + \frac{\ln\left(\frac{r_{co1}}{r_{ci1}}\right)}{2\pi L k_{csg1}} + \frac{1}{2\pi r_{co1} L h_{ca2}} + \frac{\ln\left(\frac{r_{co2}}{r_{ci2}}\right)}{2\pi L k_{csg2}} + \frac{1}{2\pi r_{co2} L h_{ca3}} + \frac{\ln\left(\frac{r_{co3}}{r_{ci3}}\right)}{2\pi L k_{csg3}} + \frac{\ln\left(\frac{r_{wb3}}{r_{co3}}\right)}{2\pi L k_{cem3}} \quad \text{Eq. 5.6}$$

$$U_{ti3} = \frac{1}{R_{total3} A_{ti}}$$

$$U_{ti3} = \left[\frac{1}{h_{ti}} + \frac{r_{ti} \ln\left(\frac{r_{to}}{r_{ti}}\right)}{k_{tbg}} + \frac{r_{ti}}{r_{to} h_{ca1}} + \frac{r_{ti} \ln\left(\frac{r_{co1}}{r_{ci1}}\right)}{k_{csg1}} + \frac{r_{ti}}{r_{co1} h_{ca2}} + \frac{r_{ti} \ln\left(\frac{r_{co2}}{r_{ci2}}\right)}{k_{csg2}} + \frac{r_{ti}}{r_{co2} h_{ca3}} + \frac{r_{ti} \ln\left(\frac{r_{co3}}{r_{ci3}}\right)}{k_{csg3}} + \frac{r_{ti} \ln\left(\frac{r_{wb3}}{r_{co3}}\right)}{k_{cem3}} \right]^{-1} \quad \text{Eq. 5.7}$$

5.2.2.4 Section 4 (casing shoe 4 to casing shoe 5)

Section 4 consist of the following resistances, left to right:

- i. The thin stagnant fluid film on the inside of the production tubing
- ii. The tubing wall
- iii. The fluid in annulus 1
- iv. The casing 1 wall
- v. The fluid in annulus 2

- vi. The casing 2 wall
- vii. The fluid in annulus 3
- viii. The casing 3 wall
- ix. The cement 3 sheath
- x. The casing 4 wall
- xi. The cement 4 sheath

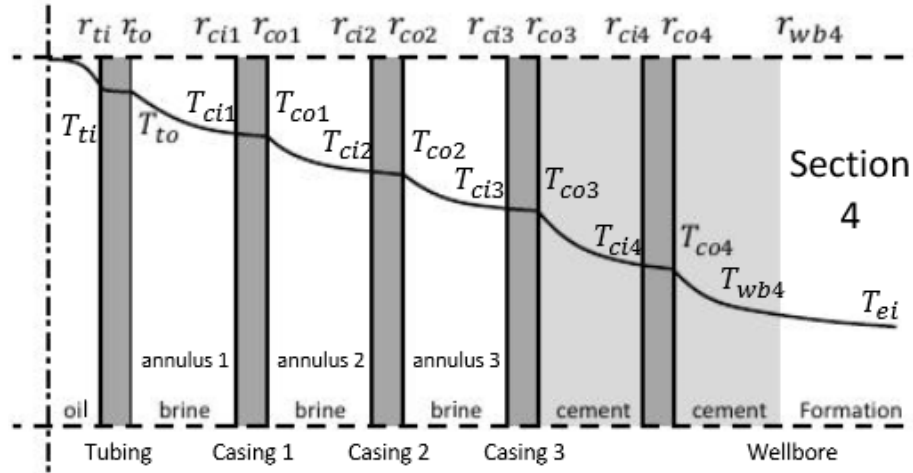


Figure 5.5: Temperature distribution throughout the wellbore cross section for section 4 [13]

$$R_{total4} = \frac{1}{2\pi r_{ti} L h_{ti}} + \frac{\ln\left(\frac{r_{to}}{r_{ti}}\right)}{2\pi L k_{tbg}} + \frac{1}{2\pi r_{to} L h_{ca1}} + \frac{\ln\left(\frac{r_{co1}}{r_{ci1}}\right)}{2\pi L k_{csg1}} + \frac{1}{2\pi r_{co1} L h_{ca2}} + \frac{\ln\left(\frac{r_{co2}}{r_{ci2}}\right)}{2\pi L k_{csg2}} + \frac{1}{2\pi r_{co2} L h_{ca3}} + \frac{\ln\left(\frac{r_{co3}}{r_{ci3}}\right)}{2\pi L k_{csg3}} + \frac{\ln\left(\frac{r_{ci4}}{r_{co3}}\right)}{2\pi L k_{cem3}} + \frac{\ln\left(\frac{r_{co4}}{r_{ci4}}\right)}{2\pi L k_{csg4}} + \frac{\ln\left(\frac{r_{wb4}}{r_{co4}}\right)}{2\pi L k_{cem4}} \quad \text{Eq. 5.8}$$

$$U_{ti4} = \frac{1}{R_{total4} A_{ti}}$$

$$U_{ti4} = \left[\frac{1}{h_{ti}} + \frac{r_{ti} \ln\left(\frac{r_{to}}{r_{ti}}\right)}{k_{tbg}} + \frac{r_{ti}}{r_{to} h_{ca1}} + \frac{r_{ti} \ln\left(\frac{r_{co1}}{r_{ci1}}\right)}{k_{csg1}} + \frac{r_{ti}}{r_{co1} h_{ca2}} + \frac{r_{ti} \ln\left(\frac{r_{co2}}{r_{ci2}}\right)}{k_{csg2}} + \frac{r_{ti}}{r_{co2} h_{ca3}} + \frac{r_{ti} \ln\left(\frac{r_{co3}}{r_{ci3}}\right)}{k_{csg3}} + \frac{r_{ti} \ln\left(\frac{r_{ci4}}{r_{co3}}\right)}{k_{cem3}} + \frac{r_{ti} \ln\left(\frac{r_{co4}}{r_{ci4}}\right)}{k_{csg4}} + \frac{r_{ti} \ln\left(\frac{r_{wb4}}{r_{co4}}\right)}{k_{cem4}} \right]^{-1} \quad \text{Eq. 5.9}$$

5.2.2.5 Section 5 (casing shoe 5 wellhead)

Section 5 consist of the following resistances, left to right:

- i. The thin stagnant fluid film on the inside of the production tubing
- ii. The tubing wall
- iii. The fluid in annulus 1
- iv. The casing 1 wall
- v. The fluid in annulus 2
- vi. The casing 2 wall
- vii. The fluid in annulus 3
- viii. The casing 3 wall
- ix. The cement 3 sheath
- x. The casing 4 wall
- xi. The cement 4 sheath
- xii. The casing 5 wall
- xiii. The cement 5 sheath

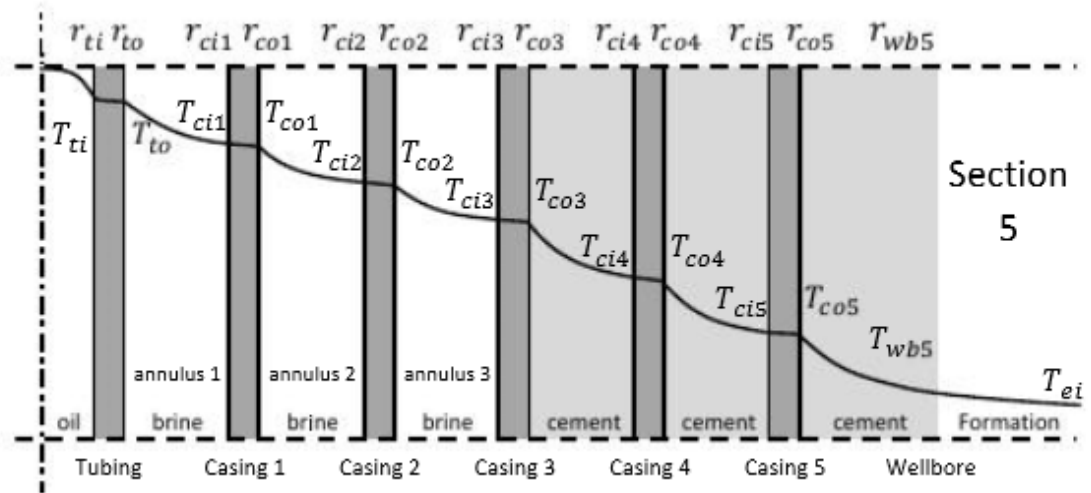


Figure 5.6: Temperature distribution throughout the wellbore cross section for section 5 [13]

$$\begin{aligned}
 R_{total5} = & \frac{1}{2\pi r_{ti} L h_{ti}} + \frac{\ln\left(\frac{r_{to}}{r_{ti}}\right)}{2\pi L k_{tbg}} + \frac{1}{2\pi r_{to} L h_{ca1}} + \frac{\ln\left(\frac{r_{co1}}{r_{ci1}}\right)}{2\pi L k_{csg1}} + \frac{1}{2\pi r_{co1} L h_{ca2}} \\
 & + \frac{\ln\left(\frac{r_{co2}}{r_{ci2}}\right)}{2\pi L k_{csg2}} + \frac{1}{2\pi r_{co2} L h_{ca3}} + \frac{\ln\left(\frac{r_{co3}}{r_{ci3}}\right)}{2\pi L k_{csg3}} + \frac{\ln\left(\frac{r_{ci4}}{r_{co3}}\right)}{2\pi L k_{cem3}} \\
 & + \frac{\ln\left(\frac{r_{co4}}{r_{ci4}}\right)}{2\pi L k_{csg4}} + \frac{\ln\left(\frac{r_{ci5}}{r_{co4}}\right)}{2\pi L k_{cem4}} + \frac{\ln\left(\frac{r_{co5}}{r_{ci5}}\right)}{2\pi L k_{csg5}} + \frac{\ln\left(\frac{r_{wb5}}{r_{co5}}\right)}{2\pi L k_{cem5}}
 \end{aligned}
 \tag{Eq. 5.10}$$

$$U_{ti5} = \frac{1}{R_{total5}A_{ti}}$$

$$U_{t15} = \left[\frac{1}{h_{ti}} + \frac{r_{ti} \ln\left(\frac{r_{to}}{r_{ti}}\right)}{k_{tbg}} + \frac{r_{ti}}{r_{to}h_{ca1}} + \frac{r_{ti} \ln\left(\frac{r_{co1}}{r_{ci1}}\right)}{k_{csg1}} + \frac{r_{ti}}{r_{co1}h_{ca2}} + \frac{r_{ti} \ln\left(\frac{r_{co2}}{r_{ci2}}\right)}{k_{csg2}} \right. \\ \left. + \frac{r_{ti}}{r_{co2}h_{ca3}} + \frac{r_{ti} \ln\left(\frac{r_{co3}}{r_{ci3}}\right)}{k_{csg3}} + \frac{r_{ti} \ln\left(\frac{r_{ci4}}{r_{co3}}\right)}{k_{cem3}} + \frac{r_{ti} \ln\left(\frac{r_{co4}}{r_{ci4}}\right)}{k_{csg4}} \right. \\ \left. + \frac{r_{ti} \ln\left(\frac{r_{ci5}}{r_{co4}}\right)}{k_{cem4}} + \frac{r_{ti} \ln\left(\frac{r_{co5}}{r_{ci5}}\right)}{k_{csg5}} + \frac{r_{ti} \ln\left(\frac{r_{wb5}}{r_{co5}}\right)}{k_{cem5}} \right]^{-1} \quad \text{Eq. 5.11}$$

Chapter 6

6 Sensitivity Analysis

6.1 Introduction

In this chapter, correlations developed in Chapter 4 for the thermophysical parameters of the various wellbore components are tested with the temperature model developed. In order to determine the parameters that affect temperature distribution and the extent of their influence, a parameter sensitive analysis is performed, based on exploring the temperature of the fluid within the tubing. A base case scenario is set to serve as a reference point for comparisons. Specifically, the effect of different cement types, annular and produced fluids, casing and tubing materials and formation types are studied against the temperature profiles.

6.2 Base Case

The base case model has crude oil as production fluid, annular fluid to be salt water, casing and tubing materials to be Stainless Steel 316, and G-class as the cement system. The formation is considered homogenous and to be sandstone. Experimental parameters for sandstone (system S1 according to their classification) by Koňáková et al (2013) [35] are used. Table 8 lists model parameters used in the base case. Figure 6.1 shows the temperature profiles plot resulting from the base case properties. The overall heat transfer coefficient profile for the base case is shown in Figure. 6.2. From Fig. 6.2 it is evident that the heat transfer is largest in the deeper parts of the well.

Table 8: Base case parameters

Parameter		Value	Units
Formation (Sandstone) [35]	ρ_e	2182.99	$[kgm^{-3}]$
	k_e	Eq. 4.26	$[Wm^{-1}k^{-1}]$
	C_{pe}	672.62	$[Jkg^{-1}K^{-1}]$
Cement:	k_e	Eq. 4.1	$[Wm^{-1}k^{-1}]$
Casing/Tubing	k_e	Eq. 4.5	$[Wm^{-1}k^{-1}]$
Geothermal gradient	gG	0.0455	$[deg/m]$
Surface formation temperature	T_e	15	$[^{\circ}C]$
Produced fluid (crude oil) Section(4.4.1)	$\rho_{o,sc}$	800	$[kgm^{-3}]$
	Flowrate, sc	0.01736 (1500)	$[m^3s^{-1}](m^3d^{-1})$
	ρ_o	Eq. 4.7	$[kgm^{-3}]$
	k_o	Eq. 4.9	$[Wm^{-1}k^{-1}]$
	C_{p0}	Eq. 4.10	$[Jkg^{-1}K^{-1}]$
	μ_o	Eq. 4.11	cP
Annular Fluid (salt water) Section (4.4.4)	ρ_{sw}	Eq. 4.21	$[kgm^{-3}]$
	K_{sw}	Eq. 4.22	$[Wm^{-1}k^{-1}]$
	C_{psw}	Eq. 4.23	$[Jkg^{-1}K^{-1}]$
	μ_{sw}	Eq. 4.25	$[cP]$
Production time	t	48	Hours (172800s)
Inclination	θ	0	[deg]

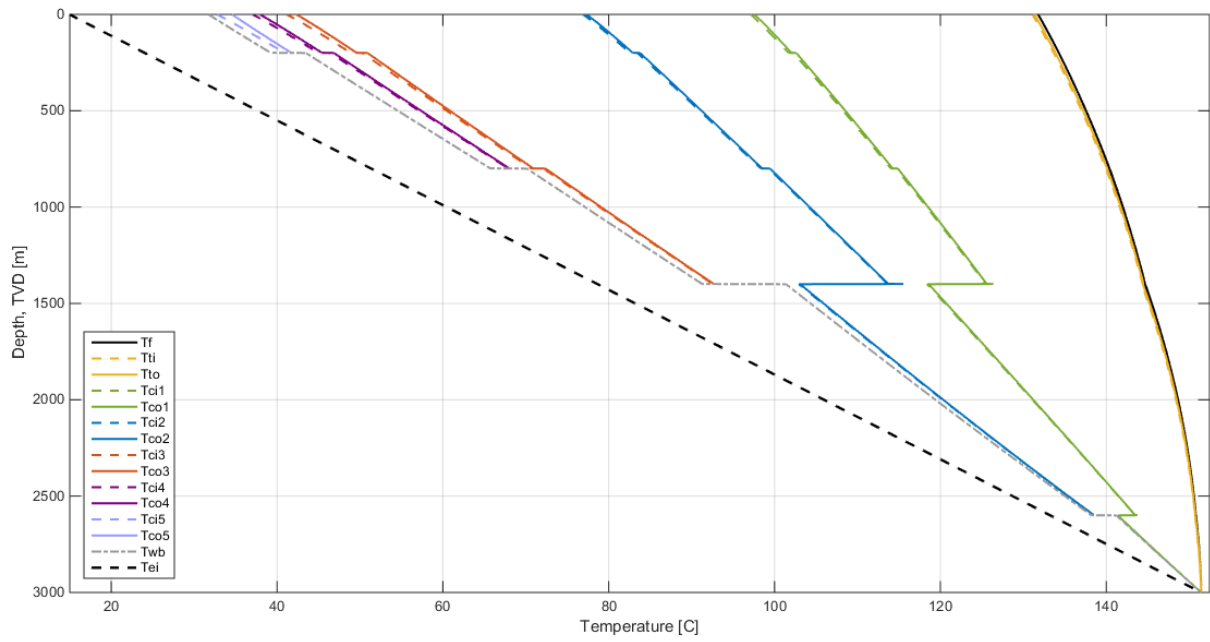


Figure 6.1: Temperature profile of wellbore (Basecase)

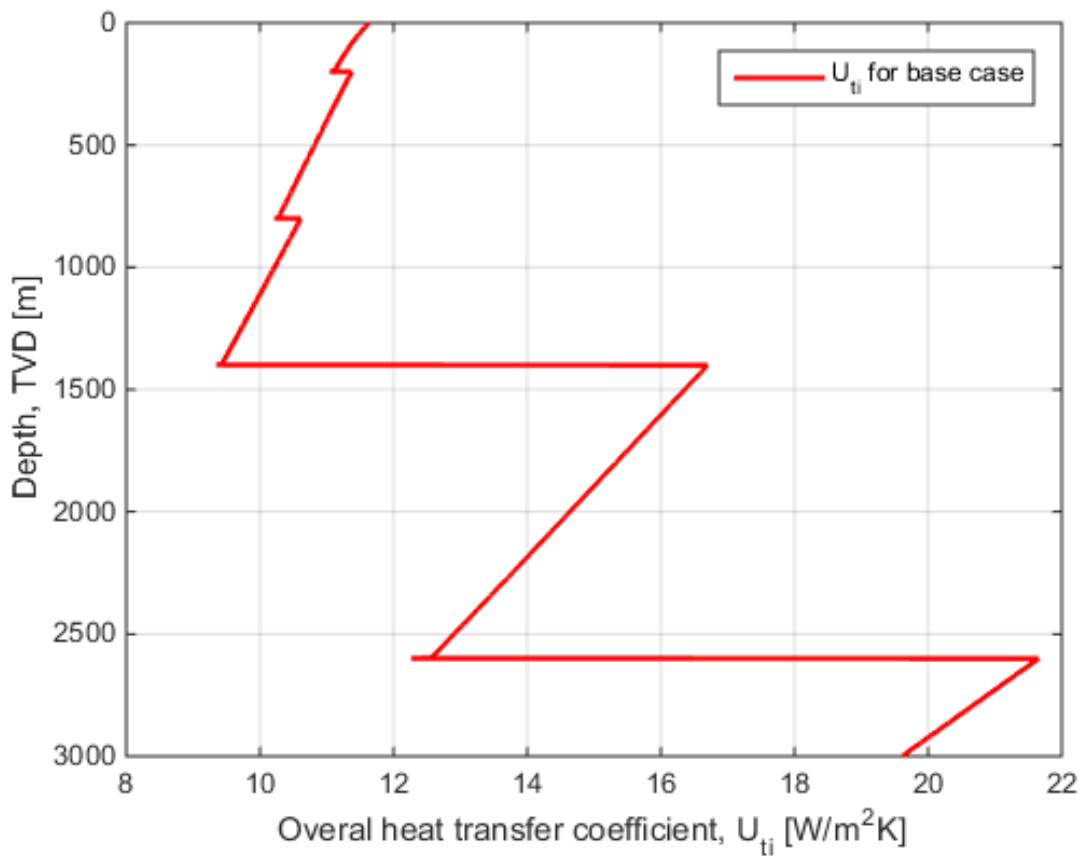


Figure 6.2: Overall heat transfer coefficient against depth for wellbore (Basecase)

6.3 Effect of Fluid Flowrate

The effect of production fluid volumetric flowrate on fluid temperature (T_f) was investigated. The flowrate was varied from 50, 300, 700, 2000 and 4500 m^3/day . As evident from the graph (Figure 6.3), the fluid temperature reduces significantly (higher rate) for lower flowrates. As the flowrate decreases, rate of fluid temperature loss within the tubing increases. This could be explained by the fact that at lower flowrates, the fluid in the tubing has a longer residence time, therefore losing more heat to the surroundings, thus the duration of the external heat transfer for fluid within the tubing is prolonged during flow. A comparison with the work by Mu et al (2018) [36] show a similar observation (Figure 6.4). In their work, they set a base case mass flowrate of 8.31kg/s and shifted it up by 20%, 40% and 60%.and down by same percentages.

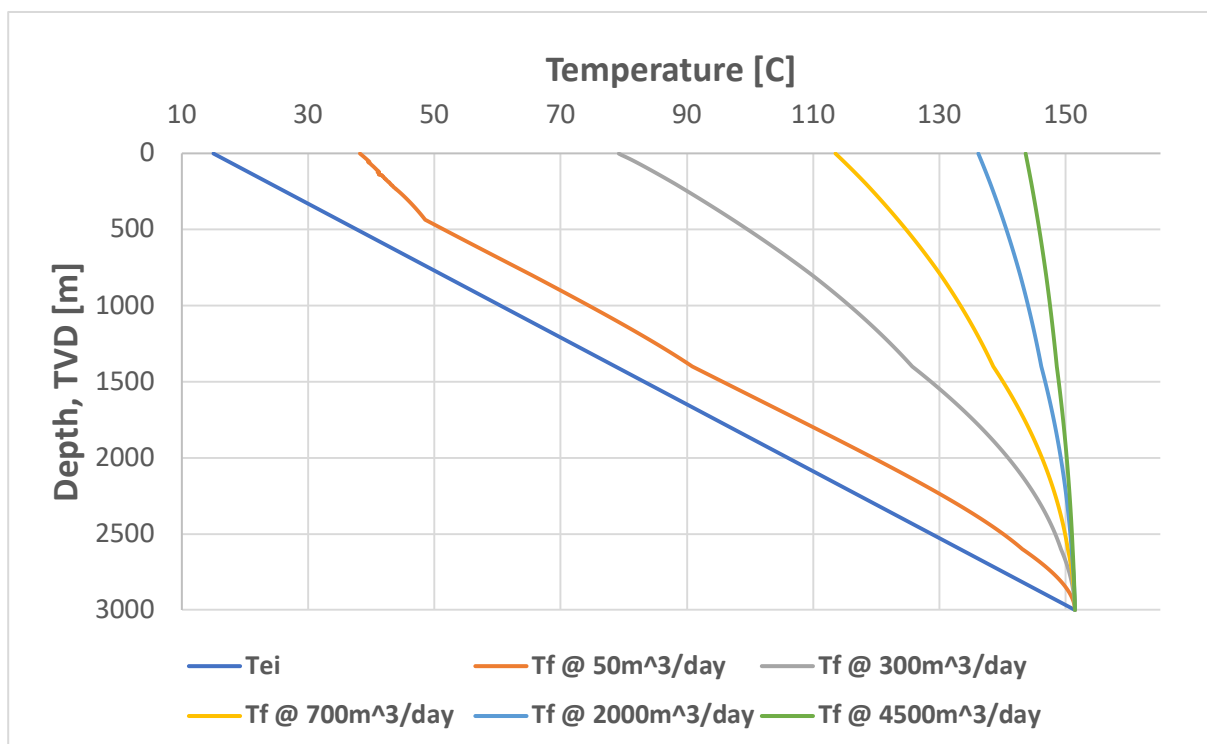


Figure 6.3: Effect of fluid flowrate on produced fluid temperature

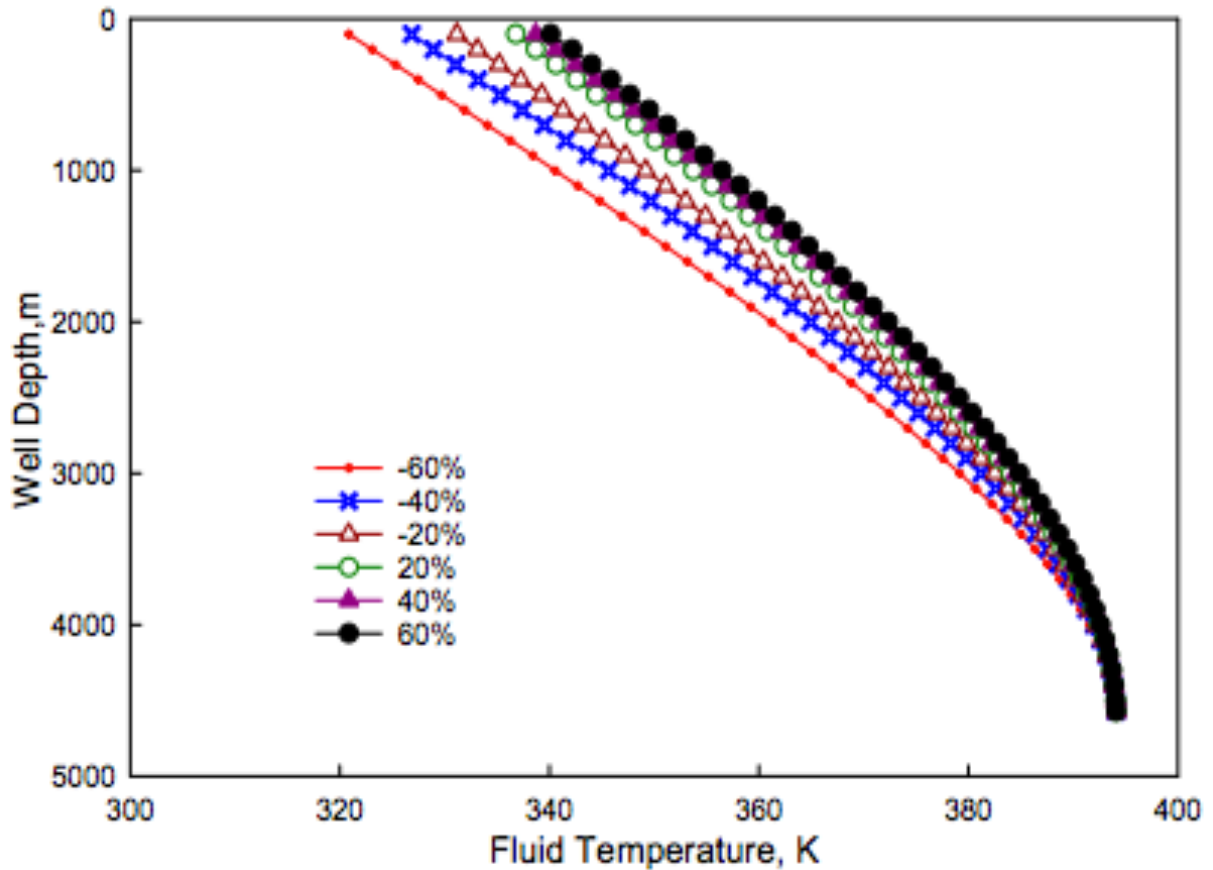


Figure 6.4 Effect of oil flow rate on the temperature distribution curve in the tubing [36]

6.4 Effect of Production time

Figure 6.5 shows the effect of production time. The time was varied in the following steps (hours): 5, 48, 100, 1000, 10000. The rate of fluid temperature reduction is lower for higher production times. This is because, the temperature of the fluid increases with depth and as time goes, hotter fluids are produced from greater depths. Generally the effect of time on the produced fluid temperature is minimal and for much higher production times, the difference in the temperature profile decreases.

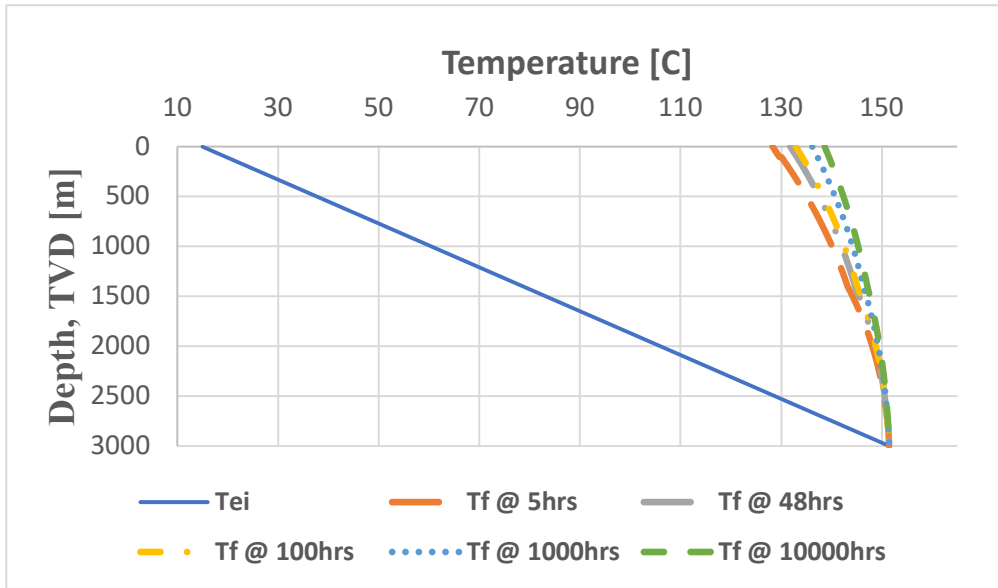


Figure 6.5: Effect of production time on produced fluid temperature

6.5 Effect of Cement Type

Three different polymers were tested namely, W50, Flyash and GGBFS. From figure 6.6, both GGBFS and W50 were much closer to the base case temperature profile. However, fluid temperature loss with flyash was very small. On the face of this graph one can conclude that, flyash will provide better thermal resistance. Figure 6.7 shows the various overall heat (U_t) transfer coefficients for the cement systems. Flyash had the lowest U_t which means its resistance to heat transfer is high.

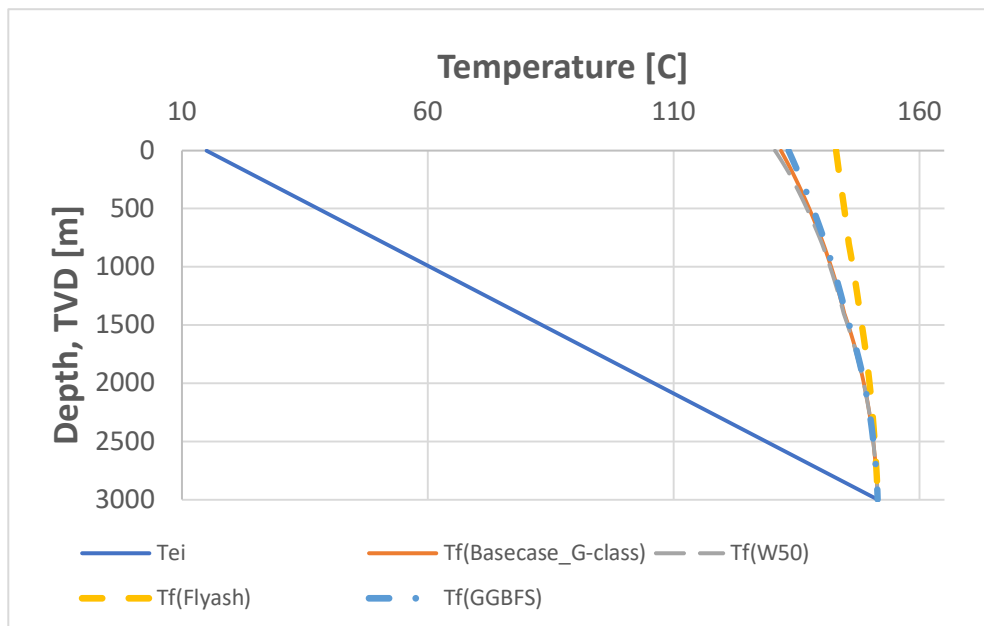


Figure 6.6: Effect of cement type on fluid temperature

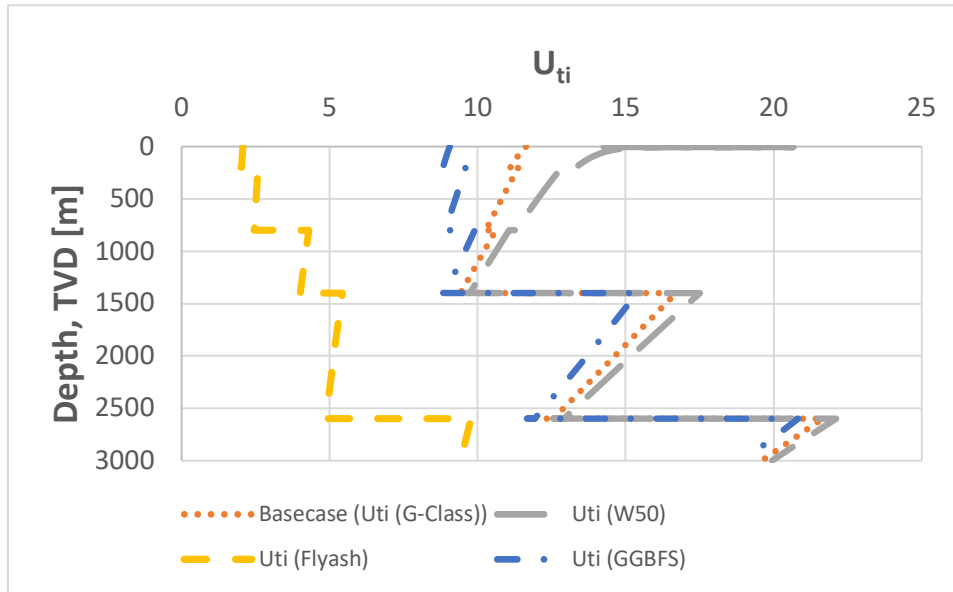


Figure 6.7: Effect of cement type on U_{ti}

6.6 Effect of Annular Fluid

Salt water (3.5% dissolved salt by weight) used as the annular fluid in the base case was changed to distilled water and then to water based mud. From Figure 6.8, the salt water maintains a higher temperature than the distilled water and water based mud. This is because of the low heat capacity of salt water compared to deionized water. Since heat capacity is the amount of heat energy it requires to heat a gram of material by Kelvin degree, the higher the heat capacity, the more slowly the distilled water will heat, given the same amount of energy added. The overall heat transfer is shown Figure 6.9.

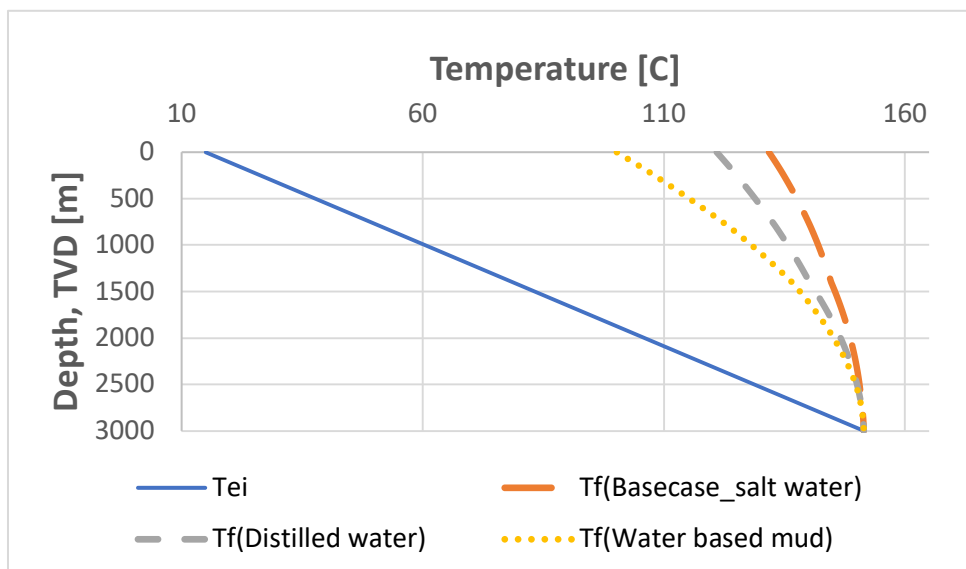


Figure 6.8: Effect of annular fluid on fluid temperature.

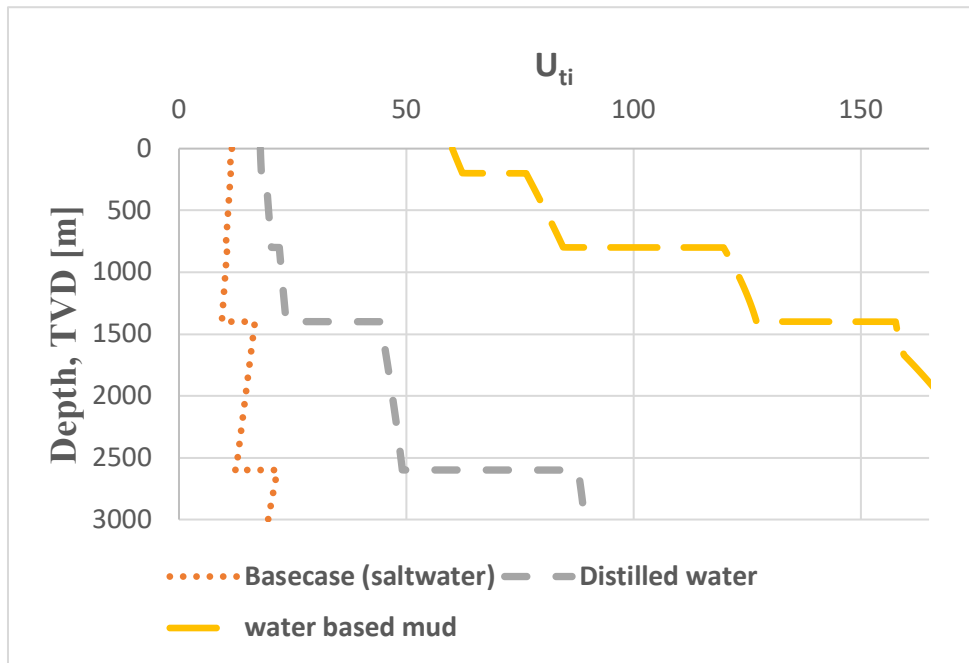


Figure 6.9: Effect of annular fluid on overall heat transfer coefficient

6.7 Effect of Produced Fluid

When the fluid in the tubing for the base case was replaced with distilled water, the temperature of the water was higher with minimal heat loss from the bottom to the surface of the wellbore. The rate of heat flow from the produced fluid to the surroundings will normally be determined by the thermal conductance of the surrounding tubing and other barriers but these barriers and their properties remain constant for both fluid systems, thus crude oil and distilled water. Also forced convection could lead to heat loss, but again the same flowrate is used in both cases. However, since the water has a higher specific heat than most oils, it would have to lose more heat to cool down compared to crude oil which explains the observation in Figures 6.10 and 6.11

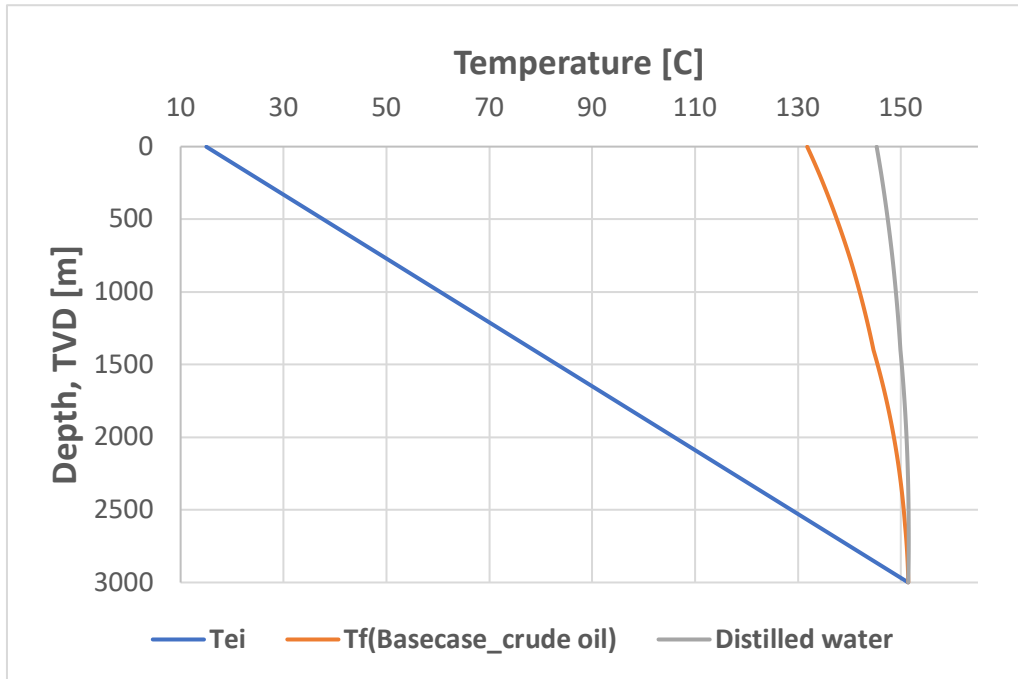


Figure 6.10: Effect of produced fluid on temperature profile

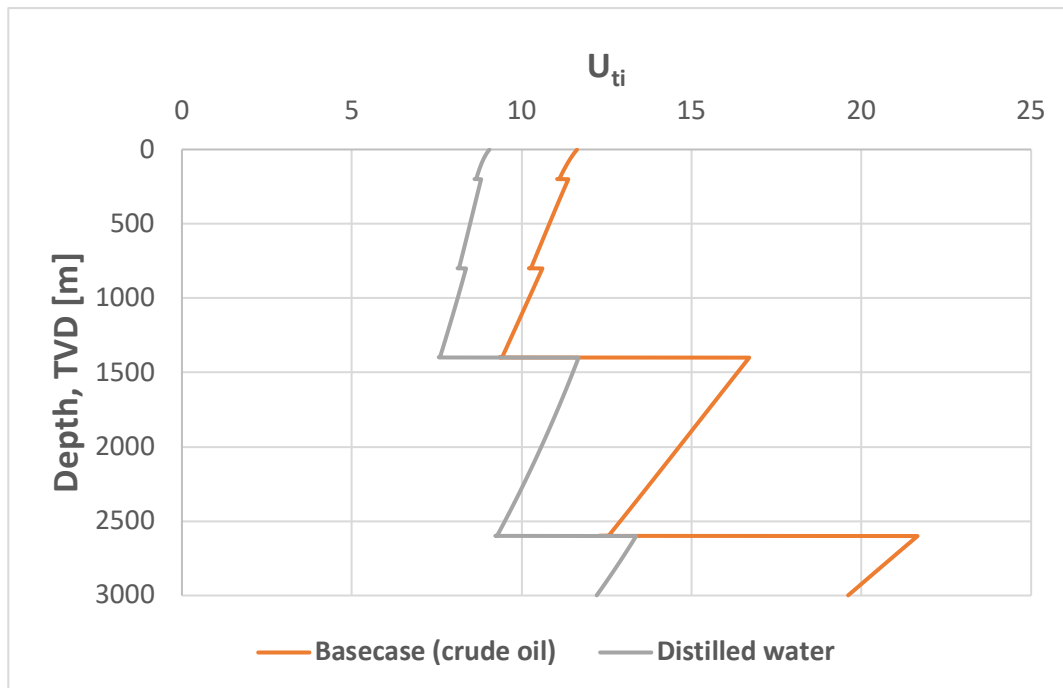


Figure 6.11: Effect of produced fluid on overall heat transfer coefficient

6.8 Effect of Casing/Tubing Material

Two grades of steel were used for the casing materials; Steel 316 for the base case and ST52. The casing conducts heat from the fluid but from Figures 6.12 and 6.13, there wasn't much difference from the two casing materials with regards to their effect on the temperature profile and overall heat transfer coefficient.

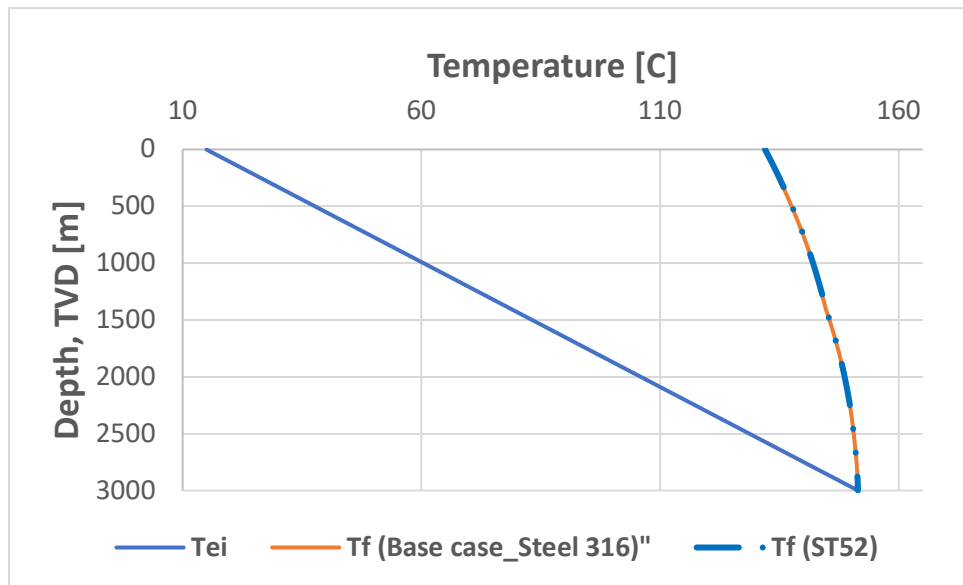


Figure 6.12: Effect of Casing material on temperature profile

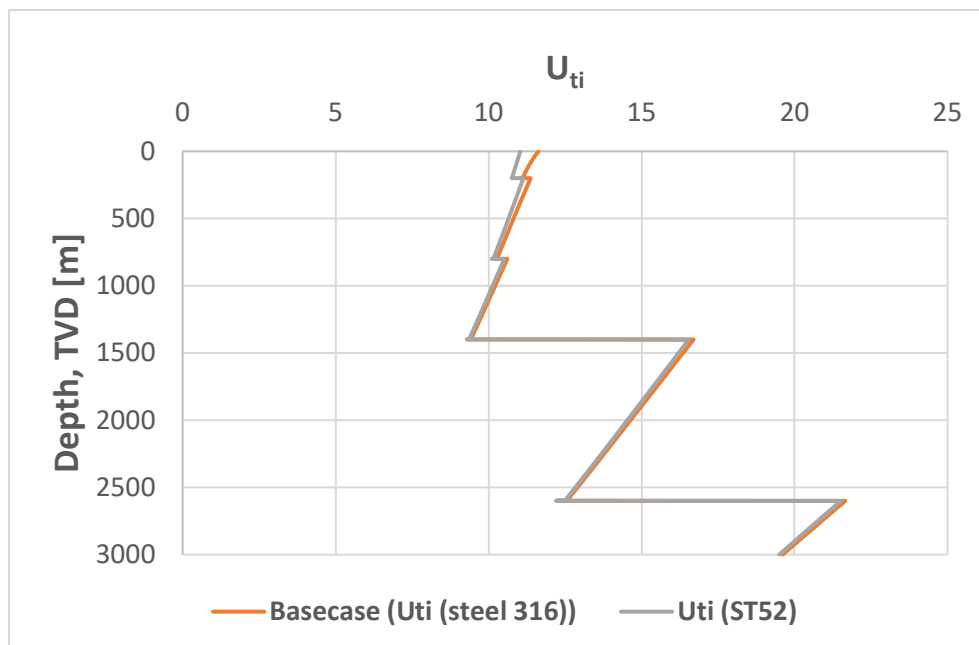


Figure 6.13: Effect of casing material on overall heat transfer coefficient

Chapter 7

7 Summary of Work and Conclusion

7.1 Summary of Work

In this study, experiments were performed using the C-Therm TCiTM thermal conductivity analyzer and Tenney Junior Test ChamberTM to measure the thermophysical parameters of wellbore components, specifically, thermal conductivity, effusivity and specific heat capacity. For production fluid, single phase crude oil and single phase distilled water were studied while for annular fluids, salt water, water based mud and distilled water were used separately at different instances. The material for the casing and tubing were considered to be same. Two grades of steel were used which were Steel 316 and ST52. Four cement systems were considered, G-Class, W50, Fly ash and Ground Granulated Blastfurnace Slag (GGBFS) and three formation types were tested, namely Berea Sandstone, Bentheimer Sandstone and Chalk. Linear and polynomial correlations were derived and implemented into a temperature model for production wells. The correlations were verified against already published work and they showed good conformance. The temperature model used had been developed but not verified with real data, so this work partly sought to perform that objective.

The temperature model is for a single phase production scenario capable carrying out a cell-by-cell piecewise calculation procedure, able to consider complex well configurations, a simple inclined wellbore trajectory, varying properties of annular and produced fluids, temperature and pressure dependence of thermophysical parameters, and natural convection in multiple annulus. Given that the overall heat transfer coefficient is found, the model is able to estimate the temperature of the produced fluid and the temperatures at all interfaces in the well configuration, also taking into consideration the Joule-Thomson heating effect on the produced fluid temperature.

7.2 Conclusion

A number of challenges were faced during measurement of the thermophysical parameters, which might have affected the results in one way or the other. This was expected as it was an experimental procedure. Any errors arising could be attributed to experimental errors,

parameters standard conditions and equipment calibration. In one instance, the result results for saltwater had to be discarded from the main work as the repeated experiments showed no conformance. The results is reported in the appendix, and results from an already published work adopted to run the sensitivity analysis.

In general the linear and polynomial correlations agreed to a large extent with published works and the following conclusions are drawn from the sensitivity studies;

1. As the flowrate of the produced fluid increases, the rate of heat loss of the fluid decreases. The flowrate was seen to have great effect on the fluid temperature profile compared to other sensitivity parameters studied (**Figure 6.1**).
2. The rate of fluid temperature reduction is lower for higher production times. Generally the effect of production time on the produced fluid temperature is minimal. **Figure (6.4)**
3. Flyash as a cement polymer provides better thermal resistance than the other cement systems (G-class, GGBFS and W50). This is because the fluid temperature reduction for this system was minimal (**Figure 6.5**).
4. When crude oil was replaced with distilled water as producing fluid, the water experienced minimal heat loss from the bottom to the surface of the wellbore. Since water has a higher specific capacity heat than crude oil, the water will would have to lose more heat to cool down which explains the observation (**Figure 6 .9, 6.10**)
5. For the casing materials tested, steel 316 and ST52, very little if not negligible difference in the fluid temperature profile was observed (**Figure 6.12**).

7.3 Recommendations for further work

Moving on the following recommendations could be adopted

1. The temperature model can be further developed to include fouling effect (such as wax and asphaltene deposition) and to include multiphase fluid systems.
2. Varying formations could be modeled into the current model.

Bibliography

- [1] A. R. Hasan, C. S. Kabir and X. Wang, "A robust steady-state model for flowing-fluid temperature in complex wells," *SPE Production & Operations*, vol. 24, no. 2, pp. 269-276, 2009.
- [2] M. Schlumberger, A. A. Perebinosoff and H. G. Doll, " Temperature measurements in oil wells.," *J. Inst. Pet. Technologist*, 1936.
- [3] T. J. Nowak, "The estimation of water injection profiles from temperature surveys," *Journal of Petroleum Technology*, vol. 5, no. 8, pp. 203-212, 1953.
- [4] L. B. Lesem, F. Greytok, F. Marotta and J. J. McKetta Jr, "A method of calculating the Distribution of temperature in flowing Gas wells," *Trans, AIME* , p. 169, 1957.
- [5] J. T. Moss and P. D. White, "How to calculate temperature profiles in a water-injection well," *Oil and Gas J*, vol. 57, no. 11, p. 174, 1959.
- [6] H. J. Ramey Jr, " Wellbore heat transmission," *Journal of petroleum Technology*, vol. 14 , no. 4, pp. 427-435.
- [7] A. R. Hasan and C. S. Kabir, " Aspects of Wellbore Heat Transfer During Two-Phase Flow," *Society of Petroleum Engineers. doi:10.2118/22948-PA*, 1994.
- [8] A. R. Hasan and C. S. Kabir, "Wellbore heat-transfer modeling and applications.," *Journal of Petroleum Science and Engineering*, vol. 86, pp. 127-136, 2012.
- [9] K. Haresh, "What is Heat Transfer?," 08 2008. [Online]. Available: <https://www.brighthubengineering.com/hvac/5231-what-is-heat-transfer/>. [Accessed 04 2018].
- [10] F. Zhou and X. Zheng, "Heat transfer in tubing-casing annulus during production process of geothermal systems.," *Journal of Earth Science* , vol. 26, no. 1, 2015.
- [11] T. L. Bergman, F. P. Incropera, D. P. DeWitt and A. S. Lavine, *Fundamentals of heat and mass transfer*, John Wiley & Sons, 2011.
- [12] J. Holman, *Heat transfer*, 10th edition, Boston: McGraw-Hill Higher Education, 2010.
- [13] T. Horpestad, "An investigation into the heat transfer process in petroleum wells, and a comprehensive modeling study investigating the temperature distribution in production wells (Master's thesis, University of Stavanger, Norway).," 2017.
- [14] G. P. Willhite, "Over-all Heat Transfer Coefficients in Steam And Hot Water Injection Wells," *Society of Petroleum Engineers. doi:10.2118/1449-PA*, 1967.

- [15] NPL, "What are thermophysical properties?," Jan 2012. [Online]. Available: [http://www.npl.co.uk/reference/faqs/what-are-thermophysical-properties-\(faq-thermal\)](http://www.npl.co.uk/reference/faqs/what-are-thermophysical-properties-(faq-thermal)). [Accessed May 2018].
- [16] A. Salazar, "On thermal diffusivity," *European journal of physics*, vol. 24, no. 4, p. 351, 2003.
- [17] R. C. Dante, *Handbook of friction materials and their applications*, Woodhead Publishing, 2015.
- [18] M. Bahrami, "Forced Convection Heat Transfer," [Online]. Available: <https://www.sfu.ca/~mbahrami/ENSC%20388/Notes/Forced%20Convection.pdf>. [Accessed June 2018].
- [19] W. Pinnoo, *Experta-presentation: Characterization of thermal conductivity by the MTPS method*, 2018.
- [20] C-Therm Technologies, "TCi Operator Manual".
- [21] P. Choktaweekarn, W. Saengsoy and S. Tangtermsirikul, " A model for predicting thermal conductivity of concrete," *Magazine of Concrete Research*, vol. 61, no. 4, pp. 271-280, 2009.
- [22] J. Won, H. J. Choi, H. Lee and H. Choi, "Numerical Investigation on the Effect of Cementing Properties on the Thermal and Mechanical Stability of Geothermal Wells. ,,," *Energies*, vol. 9, no. 12, 2016.
- [23] A. J. Philippacopoulos and M. L. & Berndt, "Characterization and modeling of cements for geothermal well casing remediation," *TRANSACTIONS-GEOTHERMAL RESOURCES COUNCIL*, pp. 81-86, 2000.
- [24] Thermtest, "Thermal conductivity testing of metals at temperatures up to 200 °C," 2016. [Online]. Available: <https://thermtest.com/thermal-conductivity-testing-of-metals-at-temperatures-up-to-200-oc>. [Accessed June 2018].
- [25] D. K. Das, S. Nerella and D. Kulkarni, "Thermal properties of petroleum and gas-to-liquid products.," *Petroleum science and technology*, vol. 25, no. 4, pp. 415-425, 2007.
- [26] M. Sattarin, H. Modarresi, M. Bayat and M. Teymori, "New viscosity correlations for dead crude oils," *Petroleum & Coal*, vol. 49 , no. 2, pp. 33-39, 2007.
- [27] W. Wright, "Simple Equations to Approximate Changes to the Properties of Crude Oil with Changing Temperature," 2014. [Online]. Available: <http://www.jmcampbell.com/tip-of-the-month/2014/04/simple-equations-to-approximate-changes-to-the-properties-of-crude-oil-with-changing-temperature/>. [Accessed June 2018].

- [28] H. D. Beggs and J. R. Robinson, " Estimating the viscosity of crude oil systems," *Journal of Petroleum technology*, vol. 27, no. 9, pp. 1-140, 1975.
- [29] X. Zheng, C. Duan, Z. Yan, H. Ye, Z. Wang and B. Xia, " Equivalent circulation density analysis of geothermal well by coupling temperature.," *Energies*, vol. 10, no. 3, p. 268, 2017.
- [30] E. S.-G. S. Santoyo, A. García, G. Espinosa and S. L. Moya, "Rheological property measurement of drilling fluids used in geothermal wells," *Applied Thermal Engineering*, vol. 21, no. 3, pp. 283-302, 2001.
- [31] M. L. Ramires, C. A. Nieto de Castro, Y. Nagasaka, A. Nagashima, M. J. Assael and W. A. Wakeham, "Standard reference data for the thermal conductivity of water," *Journal of Physical and Chemical Reference Data*, vol. 24, no. 3, pp. 1377-1381, 1995.
- [32] International Association for the Properties of Water and Steam, "Viscosity of Water," 2008. [Online]. Available: <https://wiki.anton-paar.com/en/water/>. [Accessed June 2018].
- [33] M. H. Sharqawy, J. H. Lienhard and S. M. Zubair, "Thermophysical properties of seawater: a review of existing correlations and data," *Desalination and water Treatment*, vol. 16, no. 1-3, pp. 354-380, 2010.
- [34] K. G. Nayar, M. H. Sharqawy and J. H. Lienhard, " Seawater thermophysical properties library," 2016.
- [35] D. A. N. A. Koňáková, E. Vejmelková and R. O. B. E. R. T. Černý, "Thermal properties of selected sandstones," in *In Advances in modern mechanical engineering: Proceedings of the 4th International Conference on Fluid Mechanics and Heat & Mass Trasfer*, 2013.
- [36] L. Mu, Q. Zhang, Q. Li and F. Zeng, "A Comparison of Thermal Models for Temperature Profiles in Gas-Lift Wells," *Energies*, vol. 11, no. 3, p. 489, 2018.
- [37] I. M. Kutasov and L. Eppelbaum, *Pressure and Temperature Well Testing*, CRC Press,, 2015.

Appendix A

Temperature model

We consider a small control volume, dz , in the wellbore at a distance z from the top of the well ($z = 0$ at the top of the well, and $z = z_{bh}$ at the bottom of the well), spanning between z and ($z - \Delta z$). The heat transfer across the wellbore is considered constant, and the heat transfer from formation is considered transient. As the hot reservoir fluid is produced, considered single phase, it rises along the tubing. The produced fluid, assumed to be hotter than the temperature across the annulus, casing, cement and formation at all depths except at the bottom point of the well, transports heat, $Q_{(z)}$, in to the control volume at z , and heat out of the control volume, $Q_{(z-\Delta z)}$, at distance $z - dz$. The difference in heat in and out of the control volume must be equal to the amount of heat transferred to the formation.

$$Q_{in} - Q_{out} = \text{Heat transferred to the formation} \quad \text{Eq. A1}$$

The heat transferred to the formation, Q , is equal to the change in internal heat of the control volume. The heat change over dz is given as:

$$Q_{(z)} - Q_{(z-\Delta z)} = Q \quad \text{Eq. A2}$$

The energy balance for the system, assuming steady state, can be written as:

$$\begin{aligned} [(wH)_z - (wH)_{z-\Delta z}] + \frac{1}{2} [(wv^2)_z - (wv^2)_{z-\Delta z}] \\ + [z(wg\cos\theta)_z - (z - \Delta z)(wg\cos\theta)_{z-\Delta z}] = Q\Delta z \end{aligned} \quad \text{Eq. A3}$$

Where: w : Rate of mass flow per unit area [$kg s^{-1}$]

H : Fluid enthalpy [J]

v : Fluid velocity [$m s^{-1}$]

g : Gravitational accelerations, 9.81 [$m s^{-2}$]

θ : Inclination from vertical (Degrees)

Δz : Control volume length [m]

Q : Heat transferred to the formation [J]

By dividing Eq. (A3) by Δz and evaluating the expression as $\lim_{\Delta z \rightarrow 0}$, and rearranging, we obtain the following expression:

$$\frac{dH}{dz} + g \cos \theta + v \frac{dv}{dz} = \frac{Q}{w} \quad \text{Eq. A4}$$

The $\frac{Q}{w}$ expresses the heat transfer rate from the produced fluid. The generalized relation for enthalpy change is given as (Cengel et al., 2006):

$$dH = c_{pl} dT + \left[V - T \left(\frac{\partial V}{\partial T} \right)_P \right] dP \quad \text{Eq. A5}$$

Where: c_{pl} : Specific heat capacity of the produced fluid [$Jkg^{-1}K^{-1}$]

V : Specific volume, or the inverse of density of the produced fluid [m^3kg^{-1}]

The Joule-Thomson coefficient, μ_{JT} , is defined as:

$$\mu_{JT} = \left(\frac{\partial T}{\partial P} \right)_H = -\frac{1}{c_{pl}} \left[V - T \left(\frac{\partial V}{\partial T} \right)_P \right] \quad \text{Eq. A6}$$

Assuming that the fluid does not undergo any change of phase during its rise towards the surface, enthalpy for the fluid as a function of temperature and pressure is thus given by:

$$dH = c_{pl} dT - c_{pl} \mu_{JT} dP \quad \text{Eq. A7}$$

Inserting Eq. (A7) in to Eq. (A4) and rearranging to give the expression for the change of fluid temperature, T_f with depth, z :

$$\frac{dT_f}{dz} = \mu_{JT} \frac{dp}{dz} + \frac{1}{c_{pl}} \left(\frac{Q}{w} - g \cos \theta - v \frac{dv}{dz} \right) \quad \text{Eq. A8}$$

where: T_f : Temperature of the produced fluid ($^{\circ}C$)

The heat transferred from the formation to the wellbore is given as (Hasan et al., 1994):

$$Q = -\frac{2\pi k_e}{T_D} (T_{wb} - T_{ei}) \quad \text{Eq. A9}$$

where: T_{ei} : Far away undisturbed earth temperature at the considered depth ($^{\circ}C$)

T_{wb} : Temperature at the wellbore interface ($^{\circ}C$)

T_D : Dimensionless temperature

The algebraic approximation of T_D in Eq A9 is given by the continuous formation temperature approximation.

$$T_D = \ln[e^{-0.2t_D} + (1.5 - 0.3719e^{t_D})\sqrt{t_D}] \quad \text{Eq. A10}$$

Where t_D is dimensionless time, given as:

$$t_D = \frac{\alpha_e t}{r_{wb}^2} \quad \text{Eq. A11}$$

Where: α_e : Thermal diffusion of the formation [$m^2 s^{-1}$]

t : Time [s]

α_e is given as:

$$\alpha_e = \frac{k_e}{\rho_e C_{pe}} \quad \text{Eq. A12}$$

where: k_e : Thermal conductivity of formation [$Wm^{-1}K^{-1}$]

ρ_e : Density of formation [kgm^{-3}]

C_{pe} : Specific heat capacity of formation [$Jkg^{-1}K$]

The total heat transferred across the well from the wellbore interface to the tubing fluid is given as:

$$Q_{total} = -2\pi L r_{ti} U_{ti} (T_f - T_{wb}) \quad \text{Eq. A13}$$

Where: Q_{total} : Total heat flow rate per unit length of well [$J s^{-1} m^{-1}$]

r_{ti} : tubing inside area [m]

U_{ti} : Overall heat transfer coefficient based on tubing inside area [$W m^{-2} K^{-1}$]

L : Wellbore length [m]

Assuming the heat transferred from the formation to the wellbore (A9) is equal to the total heat transferred across the well from the wellbore interface to the tubing (A13), such that:

$$Q_{total} = Q = -2\pi L r_{ti} U_{ti} (T_f - T_{wb}) = -\frac{2\pi k_e}{T_D} (T_{wb} - T_{ei}) \quad \text{Eq. A14}$$

$$Q_{total} - Q = -2\pi L r_{ti} U_{ti} (T_f - T_{wb}) + \frac{2\pi k_e}{T_D} (T_{wb} - T_{ei}) = 0 \quad \text{Eq. A15}$$

Cancelling out and rearranging:

$$-r_{ti} U_{ti} T_D T_f + r_{ti} U_{ti} T_D T_{wb} + k_e T_{ei} = 0 \quad \text{Eq. A16}$$

The wellbore temperature, T_{wb} , is now given by:

$$T_{wb} = \frac{k_e T_{ei} + r_{ti} U_{ti} T_D T_f}{k_e + r_{ti} U_{ti} T_D} \quad \text{Eq. A17}$$

Inserting Eq. (A17) in to Eq. (A9) removes the T_{wb} term, yielding the following expression for total heat conducted from the formation to the produced fluid:

$$T_{wb} = \frac{k_e T_{ei} + r_{ti} U_{ti} T_D T_f}{k_e + r_{ti} U_{ti} T_D} \quad \text{Eq. A18}$$

$$Q = -\frac{2\pi k_e}{T_D} (T_{wb} - T_{ei}) \quad \text{Eq. A19}$$

$$Q = \frac{2\pi r_{ti} U_{ti} k_e}{k_e + r_{ti} U_{ti} T_D} (T_{ei} - T_f) \quad \text{Eq. A20}$$

Defining A_d as:

$$A_d = \frac{C_{pl}\omega}{2\pi} \left[\frac{k_e + (r_{ti}U_{ti}T_D)}{r_{ti}U_{ti}k_e} \right] \quad \text{Eq. A21}$$

Where: A_d : The relaxation distance [m]

The flowing fluid specific heat capacity, C_{pl} , is in the case of water cut, given as:

$$C_{pl} = \left(\frac{q_o}{q_o + q_w} \right) C_{po} + \left(1 - \frac{q_o}{q_o + q_w} \right) C_{pw} \quad \text{Eq. A22}$$

For single phase oil, assuming no water cut, $C_{pl}=C_{po}$

Equations (A20 and A21) can now be put into Eq. (A18) We get the following expression:

$$\frac{dT_f}{dz} = \frac{T_{ei} - T_f}{A_d} - \frac{g \cos \theta}{c_{pl}} + \mu_{JT} \frac{dp}{dz} - \frac{v}{c_{pl}} \frac{dv}{dz} \quad \text{Eq. A23}$$

If we now assume that the last two terms of Eq. (A23) does not vary with depth within the considered control volume, dz , we obtain the following linear differential equation:

$$\frac{dT_f}{dz} = \frac{T_{ei} - T_f}{A_d} - \frac{g \cos \theta}{c_{pl}} + \phi \quad \text{Eq. A24}$$

Where ϕ is assumed constant throughout the small control element, and given by:

$$\phi = \mu_{JT} \frac{dp}{dz} - \frac{v}{c_{pl}} \frac{dv}{dz} \quad \text{Eq. A25}$$

The Joule-Thomson coefficient, μ_{JT} , is for a single phase fluid, defined as

$$\mu_{JT} = -\frac{1}{c_{pl}} \left[V - T \left(\frac{\partial V}{\partial T} \right)_p \right] \quad \text{Eq. A26}$$

It can be expressed as:

$$\mu_{JT} = -\frac{V}{c_{pl}}(1 - T\beta) \quad \text{Eq. A27}$$

Where: V : Fluid specific volume [$m^3 kg^{-1}$]

β : Thermal expansion coefficient of the produced fluid [K^{-1}]

T : Temperature ($^{\circ}C$)

β is given as:

$$\beta = -\frac{1}{\rho} \left(\frac{\partial \rho}{\partial T} \right)_p \quad \text{Eq. A28}$$

and can be estimated by two different density values at different temperatures for constant pressure. According to Hasan et al. (2009), when considering single phase liquid flow, the product $T\beta$ in Eq. (A27) may be neglected, which would further simplify Eq. (A27):

$$\mu_{JT} \approx -\frac{1}{\rho c_{pl}} \quad \text{Eq. A29}$$

Even though the approximation of the $T\beta$ term being very small and nearly constant may be useful for simple and fast calculations, this simplification is not implemented in the model.

The ϕ parameter may now be calculated by:

$$\phi = -\frac{1}{c_{pl}} \left[V(1 - T\beta) \frac{dp}{dz} + v \frac{dv}{dz} \right] \quad \text{Eq. A30}$$

where the pressure losses up along the tubing is given by:

$$-\frac{dp}{dz} = \left(\frac{dp}{dz} \right)_{Friction} + \left(\frac{dp}{dz} \right)_{Static} + \left(\frac{dp}{dz} \right)_{Momentum} \quad \text{Eq. A31}$$

where the friction, static and momentum pressure losses are given as, respectively

$$\left(\frac{dp}{dz} \right)_{Friction} = \frac{f_D v^2 \rho}{2d} \quad \text{Eq. A32}$$

$$\left(\frac{dp}{dz}\right)_{Static} = \rho g \cos\theta \quad \text{Eq. A33}$$

$$\left(\frac{dp}{dz}\right)_{Momentum} = \rho v \frac{dv}{dz} \quad \text{Eq. A34}$$

where: f_D : Darcy-Weisbach friction factor

According to Hasan et al. (2009) the density of single phase oil does not vary significantly with depth, resulting in a negligible static-head change with depth, such that we may neglect the kinetic-energy loss term in Eq. (A25), which would lead to ϕ being approximated by:

$$\phi = \mu_{JT} \left[\left(\frac{dp}{dz}\right)_F + \left(\frac{dp}{dz}\right)_H \right] \quad \text{Eq. A35}$$

Even though this approximation yields faster calculations, it is not implemented in the model. As we are calculating from the bottom towards the top, the undisturbed formation temperature in the current cell, $T_{ei}(i)$, is equal to that of the previous cell, $(i - 1)$, minus the temperature reduction given by the geothermal gradient. The $\cos\theta$ term takes care of the inclination of the wellbore:

$$T_{ei}(i) = T_{ei}(i - 1) - g_G \cos\theta(i) dz \quad \text{Eq. A36}$$

This expression is valid for varying inclination and geothermal gradient.

Assuming all terms but T_f is staying unchanged along the length of the considered control volume, dz , Eq. (A24) can be integrated with appropriate boundary conditions applied, yielding an equation of the following form (Hasan et al., 1994):

$$T_f(i) = T_{ei}(i) + A_d(i) \left[1 - e^{-dz/A_d(i)} \right] \left(g_G \cos\theta(i) + \phi(i) - \frac{g \cos\theta(i)}{c_{pl(i)}} \right) + e^{-dz/A_d(i)} \left(T_f(i - 1) - T_{ei}(i - 1) \right) \quad \text{Eq. A37}$$

This is a bottom-up calculation, where each subsequent calculation step is based on the fluid temperature of the former step as a boundary condition. The first step starting from the bottom

of the well assumes the temperature of the produced fluid to be equal to the in-situ formation temperature, $T_f = T_{bh} = T_{ei}$, thus eliminating the last term of Eq. (A37) for the first cell.

Appendix B

Salt water Data

From the experiments, the salt water data did not conform with literature even after repeated experiments. Each repeated experiment also gave different data set with no form of conformity. The data is therefore reported in this Appendix.

From the line of best fit, we generated this correlation for the thermal conductivity of salt water as a function of temperature.

$$k_{sw} = 2 \times 10^{-5}T^3 - 0.0009T^2 - 0,01T + 0.5405 \quad \text{Eq. B1}$$

Where: k_{sw} = thermal conductivity of salt water

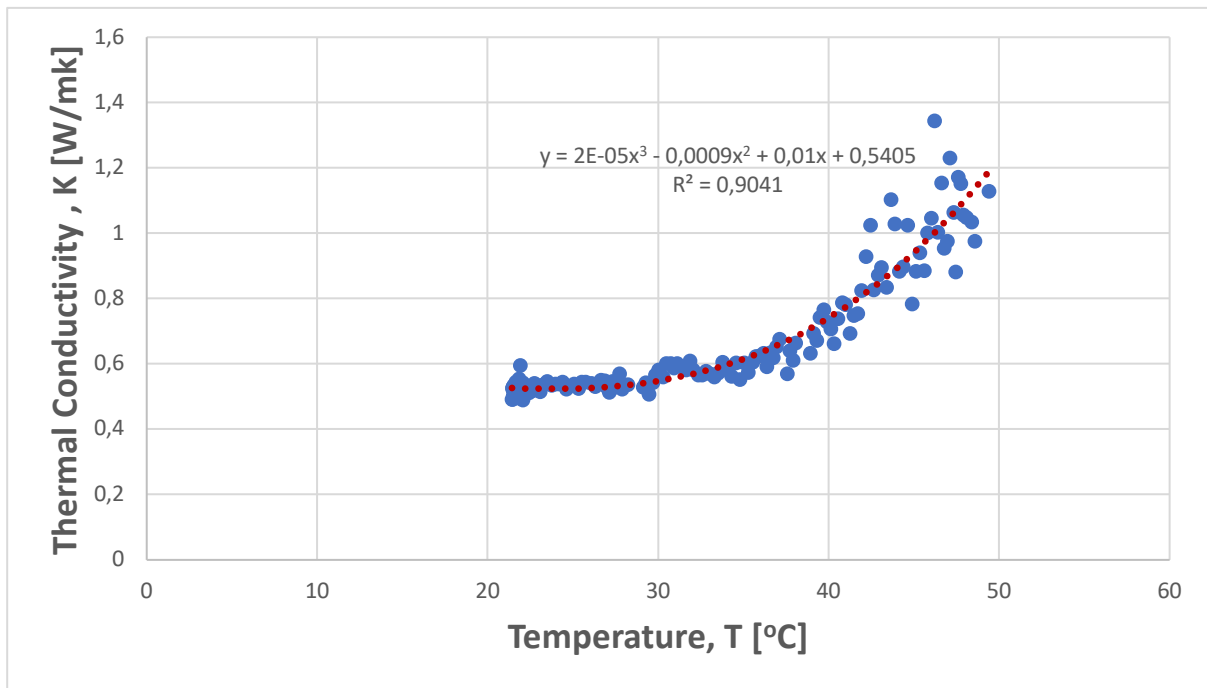


Figure B1: Thermal Conductivity of salt water (3.5%)